Please cite this paper as:

Nicolai Ababii,[1] *Mathias Hoppe,*[2] *Sindu Shree,*[2] *Alexander Vahl,*[4] *Maria Ulfa,*[3] *Thierry Pauporte,*[3] *Bruno Viana,*[3] *Vasilii Cretu,*[1] *Nicolae Magariu,*[1] *Vasile Postica,*[1] *Victor Sontea,*[1] *Oleksandr Polonskyi,*[4] *Franz Faupel,*[4] *Rainer Adelung,*[2] *Oleg Lupan,*[1,2,3*]

Effect of film thickness and noble metal functionalization on UV and gas sensing properties of sprayed TiO_2 thin films

Sensors & Actuators A: Physical **2019**, *293*, 242–258.

[1] *Department of Microelectronics and Biomedical Engineering, Technical University of Moldova, 168 Stefan cel Mare Av., MD-2004 Chisinau, Republic of Moldova*

[2] *Chair for Funtional Nanomaterials, Institute for Materials Science, Kiel University, Kaiser Str. 2, D-24143, Kiel, Germany*

[3] *Chimie ParisTech, PSL Research University, CNRS, Institut de Recherche de Chimie Paris (IRCP), 11 rue P. et M. Curie, F-75005, Paris, France*

[4] *Chair for Multicomponent Materials, Institute for Materials Science, Kiel University, Kaiser Str. 2, D-24143, Kiel, Germany*

**Corresponding authors*
Prof. Dr.Eng.Habil. Lupan,
E-mails: ollu@tf.uni-kiel.de
Institute for Materials Science, Kiel University, Germany

Keywords: TiO_2, atomic layer deposition, UV photodetector, gas sensor, gold nanoparticles

Abstract

Recently, it was established a high concern regarding environmental pollution as well as for industrial safety. Sensitive and selective detection of volatile organic compounds and H_2 gas with minimal interferences from other indoor pollutants is a critical issue for oxide gas sensors. Through this paper, we report about the effect on performance of H_2 gas sensors by varying the thickness of sensitive nanostructured TiO_2 films ranging from 12 to 40 nm accompanied with the successive functionalization with different types of noble metal nanoparticles deposited on its surface. The obtained nano- material was integrated in an electronic device for UV, gas, and gas/vapor sensing studies. Characteristics analysis revealed that the selectivity and response can be altered by the film thickness and types of noble metal nanoclusters. The results indicate that a sensor with thicker films (40 nm) of sprayed TiO_2 gives the highest response to H_2 gas (about 650%) and most stable values. The fastest response times and most rapid recovery however, were achieved with sensors having a thinner film (12 nm) of sprayed TiO_2, which also offer the highest selectivity to H_2 gas. The relatively high response (2X compared to other gases) to only H_2 gas enables the TiO_2 ultra-thin films to act as a quasi-selective sensor. The highest UV detection performances demonstrated the films functionalized with Au nanoparticles (the $I_{UV}/I_{dark} \approx 80$). The structural, chemical, electrical, UV, and gas sensing properties of such films were investigated using SEM, AFM, Raman spectroscopy, electrical characterization, and sensing experiments. It was clearly demonstrated that films are nanostructured and contains mixed phases of anatase mainly (samples annealed at 450°C for 2 h) and small of rutile after thermal annealing at higher temperatures (than 600°C for 1 h), which makes it a better nanostructured materials for sensor applications. Our study analyzes the relationship between thin film thickness, electrical properties and the gas sensing performances of such ultra-thin film (12-40 nm range) based TiO_2 gas sensors as well as the effect of different types of noble metal nanoparticles (Au, Ag, Ag-Au and Ag-Pt) deposited on its surface.

1. Introduction

Various aspects of modern daily life require the use of vapor or gas sensors. Gas chromatography and spectroscopy are highly precise techniques for gas detection and their mixtures. However, such approaches are not convenient for *in situ* sensing of gasses or vapors in fields or homeland/households places due to their size, high cost, extensive data sampling and maintenance [1,2]. In such applications high precision measurements of gas concentrations play an underlying role, the main job is to rapidly indicate on the presence of harmful or explosive gases to create a warning for surrounding people that a certain threshold has been reached. Thus, during the past decades sensors based on semiconducting metal oxide (SMO) attracted higher interest due to their smaller sizes, cost, reliability and the possibility to detect various flammable and toxic gasses, volatile organic compounds (VOCs) or just for ambient air quality monitoring [3–7]. Despite their broad spectrum of possible application areas, the selectivity and stability of SMO sensors still remains a challenge which needs further investigation but has the prospect to be improved by using new developments in this field. Some of these issues were addressed by the study of different types of oxides, including thin films and nanostructures [8–10]. TiO_2, ZnO and SnO_2 are among the most investigated SMO for sensors [8,10–14]. Due to its abundance, unique physical, electrical and chemical properties, titanium dioxide (TiO_2) thin films are among the most intensively investigated nanomaterials in this field [10,11,15–17]. Additionally, such SMO sensors are known for their longevity and robustness. TiO_2 can be found mainly in rutile and anatase (rutile-anatase (space groups: $P4_2/mnm$-$I4/amd$)) – tetragonal and brookite orthorhombic crystalline structures which differ in their properties [18,19] and are therefore of high interest for sensing applications [20,21]. TiO_2 with anatase phase is *n*-type (E_{bg} = 3.2 eV) and its electrical resistance decreases in reducing gasses, whereas the rutile phase (E_{bg} = 3.0 eV) shows *p*-type behavior [18,19]. Mazza et al [22]

demonstrated possibility to produce nanocrystalline TiO_2 thin films with controlled crystal size and anatase/rutile ratio, which makes it much more attractive for applications [20]. However, the rutile ratio greatly influences the conductivity transition, *n*-type behavior can be seen at concentrations of less than 75% rutile and *p*-type at higher concentration of rutile [18,19,23,24]. The mobility of electrical charge carriers in anatase TiO_2 is a lot larger due to the smaller effective electron mass and the higher Fermi Level compared to rutile TiO_2 [25], which makes it more desirable for gas sensor applications [18]. Several working TiO_2 based sensors for H_2, NH_3, NO_2, CO_2 and H_2O have been reported [18,26]. However, such sensor structures suffer from low selectivity which limits their practical applications. To solve some of these issues, different approaches were studied, including functionalization or decoration with noble metals on the SMO surfaces [8,10,12]. According to the most recent works, surface doping or functionalization with noble nanoparticles allows for the control of selectivity and stability of TiO_2 (and other SMO) based gas sensors, as well for improving their response value [17,27]. Noble metal nanoparticles or nanoclusters are well known for their selective adsorption of different gasses, as well as for following catalytic action to dissociate adsorbed gasses which may also improve the performances of TiO_2 based gas sensors [1–3]. Thus, the deposition of noble metal nanoparticles on the oxide surfaces increases the selectivity and sensitivity of SMO based sensors. However, it requires further and detailed investigation, since these performances are strongly affected by dimensions and shapes of the used nanoclusters. The successful deposition of noble metal nanoparticles on oxides have been reported by various techniques, like electrochemical [3], sputtering [28], sol-gel [29] and other approaches [30].

In this study, we sprayed nanostructured TiO_2 ultra-thin films on glass substrate and found that they are highly sensitive and quasi-selective to H_2 gas with low cross-responses to other VOCs such as *n*-Butanol, ethanol, etc. The main objective of this investigation was to find the optimal thickness and thermal annealing (TA) regime that enhances the selectivity and leads to a high H_2 gas response. The focus was set on noble metal functionalized TiO_2 to show how

metallic and bi-metallic nanoclusters affect the sensor performances to allow for the fabrication of more advanced sensor structures.

2. Experimental

Commercially available microscope slides (Thermo scientific, 2.5 × 7.5 cm) were used as substrate for the sensor fabrication. All slides were precleaned by an HCl dip (7%) and subsequently rinsed with deionized water, then in acetone for 10 min followed by ethanol (10 min) and water, all in ultrasonic bath cleaned. Prior each spray deposition, all glass substrate were placed on a heating plate, the temperature was set to 450°C and hold for 20 min. The spray pyrolysis was performed as reported by Pauporté et al [31]. The precursor solution used for the aerosol spray pyrolysis technique was a mixture of 0.6 mL of titanium diisopropoxide (TTIP) and 0.4 mL of acetylacetone in 7 mL of isopropanol. An Oxygen gas flux was used as carrier gas to feed the aerosol through a specially designed glass nozzle (10 mm in diameter) onto the glass substrate. The O_2 flux was fixed and the substrates remained on the heated hotplate during the deposition process. The deposited layer was then annealed at 450°C for another 60 min before allowing it to cool down naturally. The TiO_2 films thickness was controlled by regulating the spray time [31].

All sprayed TiO_2 samples were about 12 nm, 20 nm or 40 nm in thickness and were post annealed for 1 or 2 h at 450°C, 600°C or 620°C in air to stabilize the crystalline phase and decompose all residue materials from the surface. Finally, Au-contacts as interdigitated electrodes were added on top of the annealed thin films by DC-sputtering through a shadow mask with meander shape and a gap of 1.0 mm [4]. All production details for each sensor are indicated directly in the figure captions as well as in the related discussion parts to avoid confusions.

Noble metal nanoparticles (NPs), namely Ag, Au and bimetallic AgAu and AgPt nanoparticles were deposited on the spray deposited TiO_2 thin films using an custom-made Haberland type Gas Aggregation Source (GAS) [32], which is attached to a high vacuum deposition chamber [33–36].

The system was pumped below a pressure of 10^{-4} Pa prior to every deposition by a two-stage pumping system with a turbo molecular pump (Pfeiffer Vacuum, TMU 262) and a dry scroll pump (Agilent Technologies, SH-110).

The DC planar magnetron source (Thin Film Consulting, ION'X-2UHV) inside the GAS is equipped with a monometallic or bimetallic noble metal target (50 mm diameter). For the deposition of Ag and Au NPs, a monometallic target (Au: Alfa Aesar, 99.99%; Ag:Kurt J. Lesker, 99.99 %), and for the deposition of bimetallic alloy NPs, a custom built bimetallic AgAu and AgPt target is used. The samples are placed perpendicular to the nanoparticle beam at a distance of 90 mm from the exit orifice (diameter 2 mm) of the GAS. For sputtering, a flow (48 SCCM) of Ar (purity 99.999%) was supplied at the gas inlet of the GAS, resulting in a pressure inside the GAS of typically 136 Pa during deposition. For DC unipolar magnetron sputtering a DC power of 40 W (Advanced Energy, MDX 500) was supplied.

Prior to every deposition process, the target was cleaned and nanoparticle growth was conditioned for a sufficient time (at least 15 s) to reach stable deposition conditions.

The morphological, chemical, structural, and micro-Raman investigations were performed as was reported previously [3,37]. The Raman spectra were studied with an Invia Renishaw spectrometer equipped with a Leica DM2500 microscope. The excitation light was a 473 nm diode laser attenuated to about 10 mW. For better spatial resolution, a 100× objective lens with numerical aperture of 0.9 was used. The collected signal was filtered with an edge-filter cutting at about 100 cm^{-1} of the 473 nm Rayleigh line. It was dispersed with a 2400 lines/mm optical grating and the intensity was measured by a thermo-electrically cooled 1024 by 256 pixel CCD

camera, whose calibration was checked using a Si standard. Namely, for X–ray diffraction (XRD) measurements the Seifert 3000 TT unit at 40 kV and 40 mA, with graphite monochromatized $CuK_{\alpha 1}$ radiation (λ = 1.5405 Å) was used. Spray coated TiO_2 thin films with and without decoration of Ag, AgAu, AgPt and Au NPs has been investigated by X-ray photoelectron spectroscopy (XPS, Omicron Nano-Technology GmbH, Al-anode, 240W) in order to determine their chemical composition. The recorded spectra were charged referenced on the basis of the aliphatic carbon C-1s line at 285.0 eV using the software CasaXPS (version 2.3.16). [32–36].

Sensor design was performed similarly as for state of the art solid state gas detectors based on semiconducting oxides, usually with a planar structure, namely in our case a film of sensitive layer being supported by a glass/quartz substrate, then covered with Au meander electrodes for electrical connections. In the present study a planar structure thin film gas sensor was fabricated with TiO_2 sprayed films as the sensing layer. A thin sensitive TiO_2 film was deposited by a spray technique onto a glass/quartz substrate, then it was sputtered interdigitated meander shaped electrodes (electrode spacing=1 mm between Au pads).

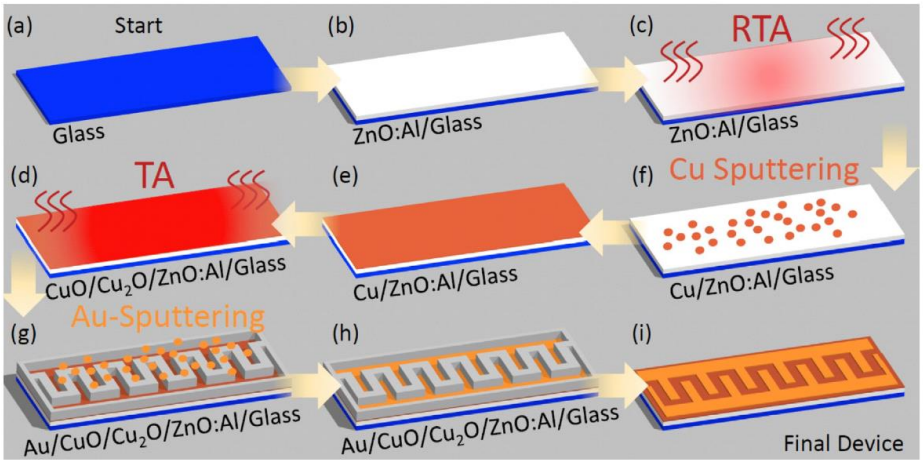

Fig. 1. The technological flow for the (CuO-Cu_2O)/ZnO:Al device fabrication based on nanostructured films. The overall process can be described as follows: (a) Starting from a glass substrate, the ZnO:Al nanostructured films are deposited via the SCS approach from aqueous solutions (at low temperatures, < 95 °C) (b), followed by a RTA treatment at individual temperatures for 60 s (c). Step one in the formation of a CuO-Cu_2O layer is the sputter deposition of a Cu thin-film followed by thermal annealing at 425 °C (d-f); the contact formation is also performed by sputtering shaded by a metal meander mask, to create a 1 mm gap (g-h). The final device structure is showed in (i).

All the gas sensitivity measurements were carried out at operating temperatures 200°C, 250°C, 300°C, 350°C and 400°C. The UV and gas sensing properties were performed as described in previous papers [7,38]. Before injecting volatile organic compounds insite 2 L testing chamber, the TiO_2 films based sensor was allowed to reach the baseline current stable value for 15 min. Once the baseline current was stabilized and hold for 15 min, then a specific amount of VOCs or H_2 test gasses were introduced into testing chamber and change of electrical current was recorded by using a Keithley 2400 with a LabView interface on a computer.

3. Results and Discussion

3.1. Morphological Properties of the TiO_2 films produced by spray pyrolysis

The films show very good adhesion to the glass substrates after months and even after more than one year. **Figure 1** depicts the SEM micrographs of undecorated TiO_2 films. From the images it can be observed that the films exhibit a uniform granular morphology with interconnected grains growth with longer thermal annealing for 2 h from 450 °C (**Figure 1a-c**), at 600°C (**Figure 1d-f**) and up to 625°C (**Figure 1g-i**). Nanocrystalline thin films were observed in all types of samples. **Figure 1j-l** shows the SEM micrographs of TiO_2 films (TA 625°C, for 2 h) decorated with Au nanoparticles investigated at low, medium and higher magnification, respectively.

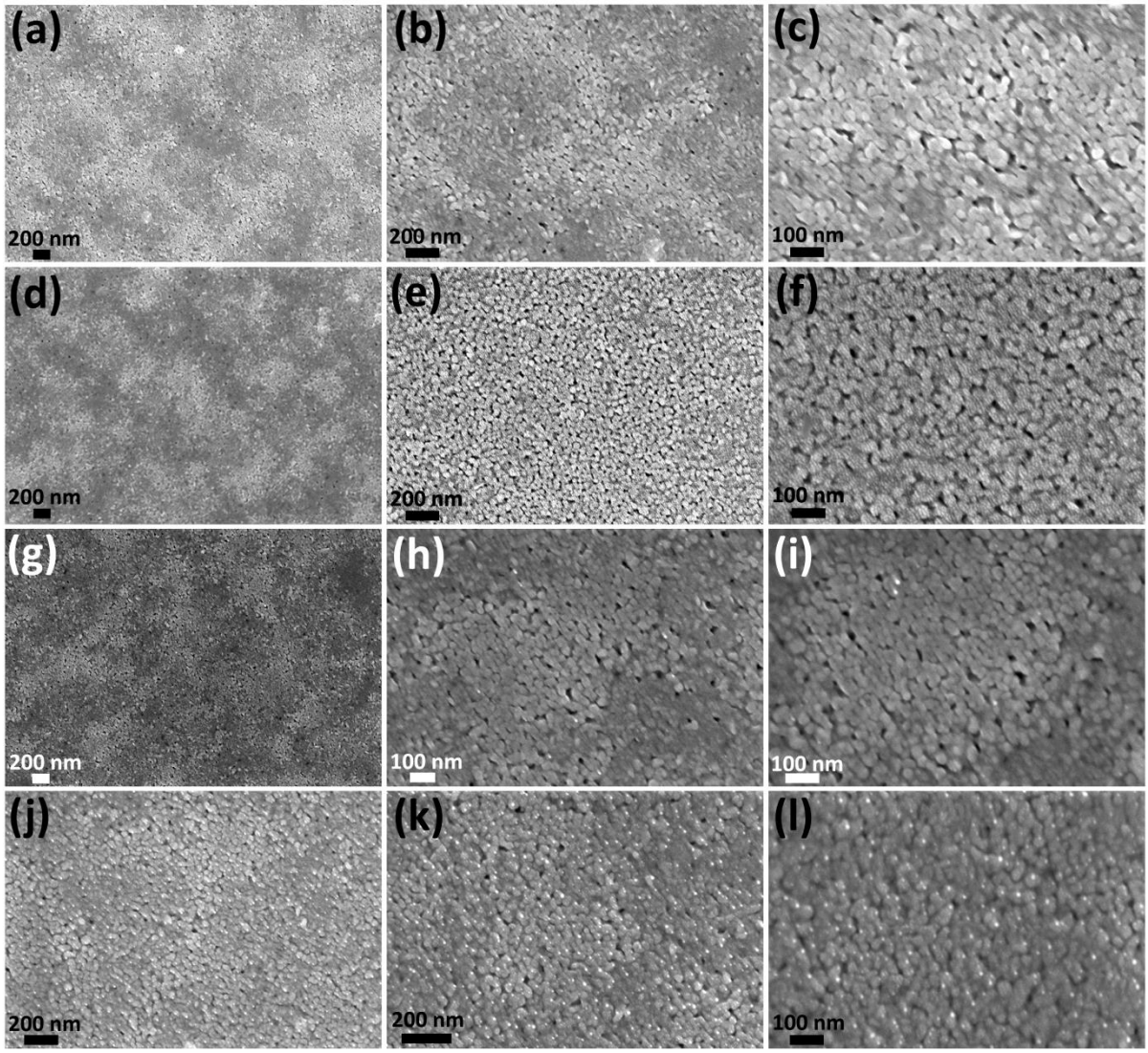

Figure 1. SEM images of nanocrystalline TiO_2 films grown by spray pyrolysis and thermally annealed at: **(a-c)** 450°C for 2 h; **(d-f)** 600°C for 1 h; **(g-i)** 625°C for 2 h; and **(j-l)** 625°C for 2 h functionalized with Au nanoparticles investigated at low, medium and higher magnification, respectively.

In the supporting information in **Figures S1a,b** a comparison of SEM micrographs of undecorated TiO_2 films at low magnification (TA at 600°C, for 1 h) with thicknesses of 20 nm and 40 nm are shown, which already indicates on a change in morphology by the increased film thickness. **Figures S2a-b** present the SEM micrographs of undecorated TiO_2 films (TA at 625°C for 2 h) which have high resemblance with cluster-assembled nanocrystalline films.

Figures S2c-d presents the SEM micrographs of TiO_2 films (TA at 600°C for 1 h) before and after surface functionalization with Au nanoparticles.

Figure 2a shows a SEM image of TiO_2 film decorated with Au nanoclusters and **Figure 2b** presents the functionalization with Ag-Au bi-metalic nanoclusters.

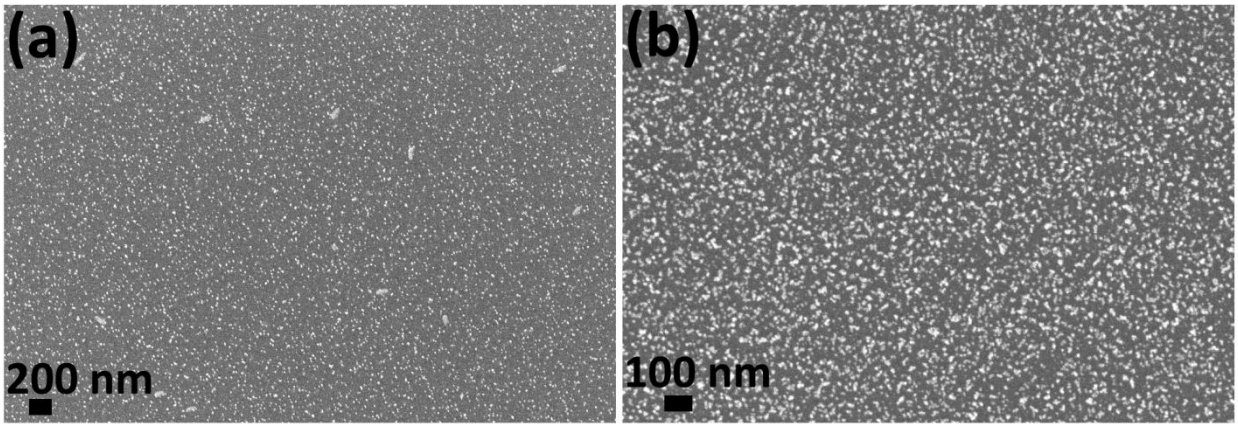

Figure 2. SEM images of TiO_2 films decorated with: **(a)** Au nanoclusters; and **(b)** Ag-Au nanoclusters.

3.2. Micro-Raman studies

The micro-Raman spectra were measured to identify the crystallization phase of TiO_2 films with different thicknesses and post-deposition annealing. All measurements were taken in dispersive mode and the excitation light was a 473 nm (10 mW) LED Laser, as described in previous papers [7,38]. Due to the resolution of the system, no distinguishable crystallization peaks were detected neither by XRD nor by Raman in the layers with a thickness of 12 nm [39].

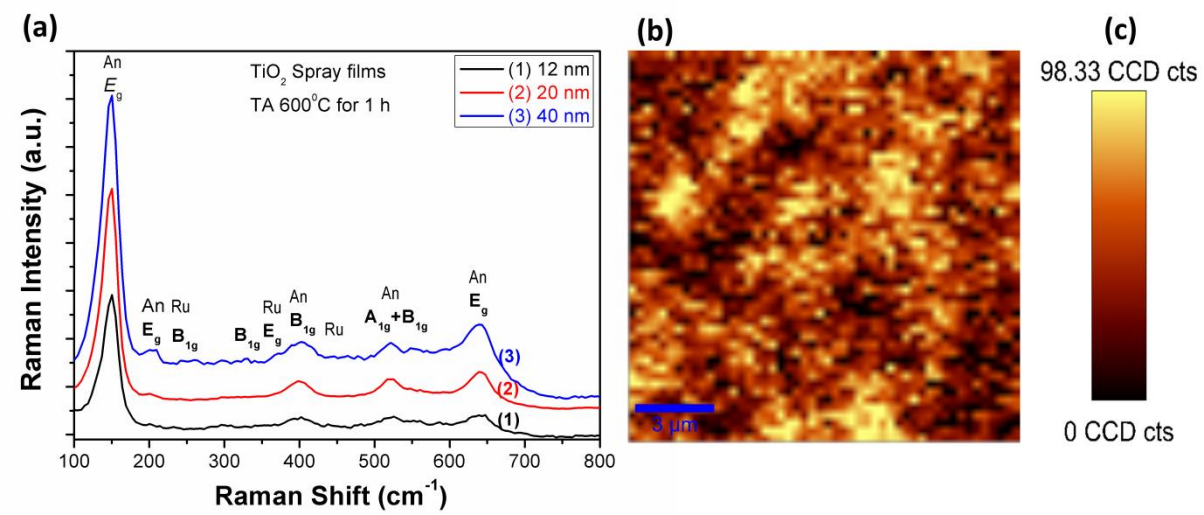

Figure 3. (a) Raman spectra of annealed nanocrystalline TiO_2 films (at 600°C for 1 h), 12 nm (spray0.5), 20 nm (spray1) and 40 nm (spray2) thickness, respectively. (b) Raman mapping of the E_g mode (144 cm^{-1}) for TiO_2 films with 40 nm thickness and TA at 600°C for 1 h.

Figure 3a represents the micro-Raman spectra of the TiO_2 films with different thicknesses (12 nm (spray0.5), 20 nm (spray1) and 40 nm (spray2) thickness, respectively) with TA at 600°C for 1 h. For the latter the Raman mapping of the E_g mode (144 cm^{-1}) is shown in **Figure 3b**. It can be clearly seen that this mode is uniformly distributed over the entire surface of the sprayed layers. **Figure S3a** represents the micro-Raman spectra of the TiO_2 films with same thickness of 40 nm but different TA conditions (450°C for 2 h, 600°C for 1 h and 625°C for 2 h). The spectra of the samples with the thickness of 20 nm and 40 nm (annealed at 450°C for 2h) were almost the same. **Figure S3a** shows only the anatase phase, which belongs to the $D_{4h}^{19}(I4/amd)$ space group [40] with two TiO_2 formula units per primitive cell. The modes at the Γ point belong to the representation [40]:

$$\Gamma_{opt} = 1A_{1g} + 1A_{2u} + 2B_{1g} + 1B_{2u} + 3E_g + 2E_u \quad (1)$$

The A_{1g}, B_{1g} and E_g modes are Raman active and the A_{2u} mode and the two E_u modes are infrared active. The peaks at ~ 144, ~ 197, ~ 326, ~ 400, ~ 513-517, and ~ 635 cm^{-1} from **Figure 3a** (curves 2-3) can be attributed to the E_g, E_g, B_{1g}, B_{1g}, A_{1g} + B_{1g}, and E_g modes of anatase, respectively [41–43]. These Raman peaks are in correlation with the anatase phase in the TiO_2 film [44].

For the rutile phase with six atoms in primitive cell there are 15 optical modes and three acoustic modes. Based on group analysis, the modes at the Γ point belong to the representation [45]:

$$\Gamma_{opt} = A_{1g} + A_{2g} + A_{2u} + 2B_{1u} + B_{1g} + B_{2g} + E_g + 3E_u \quad (2)$$

where g shows Raman active, u infrared active and E degenerate modes. The rutile phase is hard to detect due to the superimposed band at ~ 143 cm^{-1} (B_{1g}) situated close to those of the anatase phase at ~ 144 cm^{-1}, usually with low intensity [41,46]. The other Raman active modes of the rutile phase at 826 (B_{2g})(not shown here), 612 (A_{1g}) and 447 cm^{-1} (E_g) [41] were not observed in the measured Raman spectra of samples annealed at 450°C for 2 h (see **Figure S3a, curve 1**), but some traces of the rutile phase in samples annealed at higher temperatures were observed, namely 600°C for 1 h (see **Figure S4**) and 625°C for 2 h. **Figure S4** clearly shows some rutile spectral features which are present in films with higher annealing temperature (>600°C). The peaks at ~ 143, ~ 246, ~ 366, ~ 440, and ~ 610 cm^{-1} from **Figure S4** can be attributed to the B_{1g}, 246 (broad band), E_g, and A_{1g} modes of TiO_2 rutile phase, respectively [41–43]. We investigated in details more than hundred films by measuring multiple spectra at random positions on such thin film to map the size dependent changes of the Raman peaks for the anatase as well as the rutile nanostructures. The two phases are coexisting in samples annealed at higher temperatures (>600°C for 1 h, see **Figure S4**) and 625°C for 2 h and looks like they are uniformly distributed in the nanostructured films, one can say at the same time

their influence on the lattice dynamics. **Figure S3b** shows the Raman mapping of the E_g mode (144 cm^{-1}) for the TiO_2 thin films with 20 nm thickness and TA at 625°C for 2 h. It can be clearly seen that this mode is uniformly distributed over the entire surface of the sprayed layers. We can conclude that thermal annealing induced oxidation of samples is independent from the crystalline phase of nanoclusters forming these thin films.

3.3. AFM studies

Three dimensional topographic images including a roughness analysis were obtained by AFM on a 5 µm × 5 µm area from the Au-functionalized TiO_2 films. **Figure 4** shows the granular structure of an Au-functionalized TiO_2 film. The grain size is in the range of 20 - 200 nm and the surface roughness is about 2.19254 nm. Based on these AFM results we can conclude that the TiO_2 films show a quite uniform morphology.

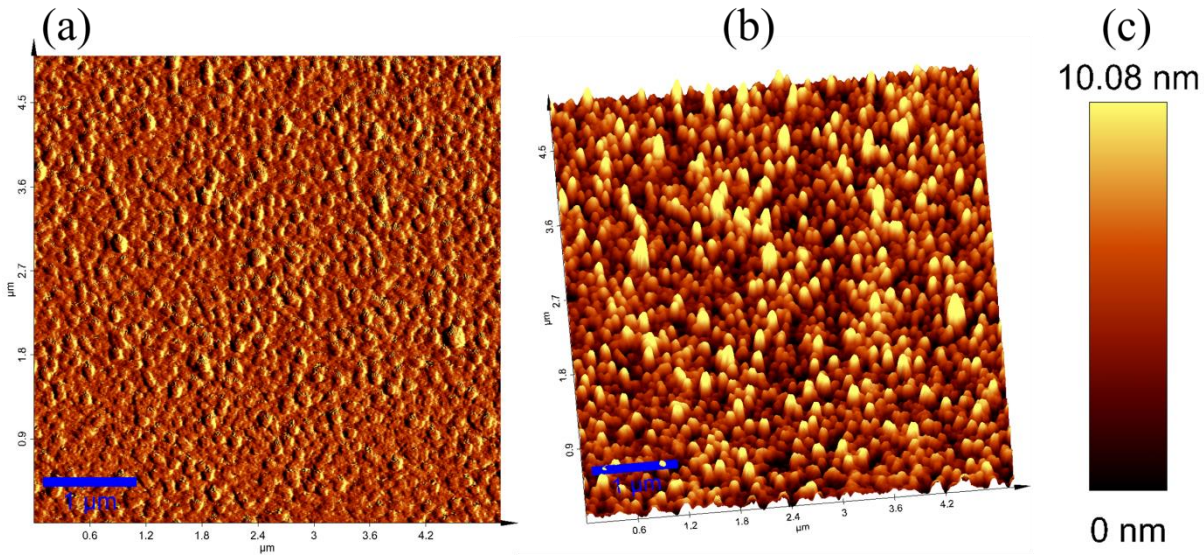

Figure 4. Surface scan by AFM in tapping mode: **(a)** Amplitude image of TiO_2 films annealed at 625°C for 2 h (inset scale bar is 1 µm; **(b)** 3D topographical image; **(c)** The scale bar of the topographical image of the deposited sample.

3.4. XPS results

An XPS investigation was conducted on the spray coated TiO_2 thin film as well as nanocomposites decorated by noble metal NPs. The overview spectra, shown in **Figure 5a**, indicate on the presence of O, C, Ca and Ti in all thin films. Ti and O originate from the spray deposited TiO_2 thin film. C and also partially O stem from atmospheric surface contamination by adsorbates on the surface. The systematic occurrence of signal corresponding to Ca indicates the migration of Ca from the used glass substrate towards the TiO_2 thin film surface. Additionally, for the NP decorated nanocomposites the characteristic lines for Ag, Au or Pt are present espectively, indicating the successful deposition of NPs onto the TiO_2 thin film surface.

For in depth analysis, high resolution spectra are presented in **Figure 5b-d**. The C-1s line at 285.0 eV was used for charge referencing of the thin films. In the TiO_2/AuNP nanocomposite, the Au-4f lines show peaks observed at 84.1 and 87.8 eV, which can be attributed to metallic gold and are in a good agreement with the XPS data reported in the literature [33,47,48]. Consequently, the deposited nanoparticles are metallic gold nanoclusters. The position of the gold peak (Au-$4f_{7/2}$ ~84.1 eV) was also used to crosscheck the binding energy calibration (charge correction) in case of the nanocomposite. The undecorated TiO_2 thin film does not show any Au signal.

The comparison of the high resolution spectra for Ti-2p lines in **Figure 5c** shows slight shifts of the Ti-$2p_{3/2}$ and Ti-$2p_{1/2}$ lines for the noble metal NP decorated nanocomposites compared to the undecorated TiO_2 thin film. A Ti-$2p_{3/2}$ peak between 459.6 eV and 458.0 eV is commonly attributed to Ti^{4+} in TiO_2, whereas lower binding energies would indicate on the presence of Ti_2O_3 (around 456.8 eV), TiO (around 455.0 eV) or metallic Ti (around 454 eV) [33,47]. For all nanocomposites the Ti-$2p_{3/2}$ peak is located between 458.9 eV and 458.3 eV, which is in good agreement with Ti^{4+} in TiO_2.

The investigated nanocomposites contain monometallic or bimetallic noble metal nanoparticles. The high resolution spectra of the corresponding Ag-3d, Au-4f and Pt-4f lines in

Figure 5d imply the successful deposition of monometallic (Ag or Au) or bimetallic (AgPt or AgAu) NPs. The quantification based on the high resolution XPS spectra indicates a Ag concentration of roughly 20% in the AgAu NPs and of roughly 80% in the AgPt NPs.

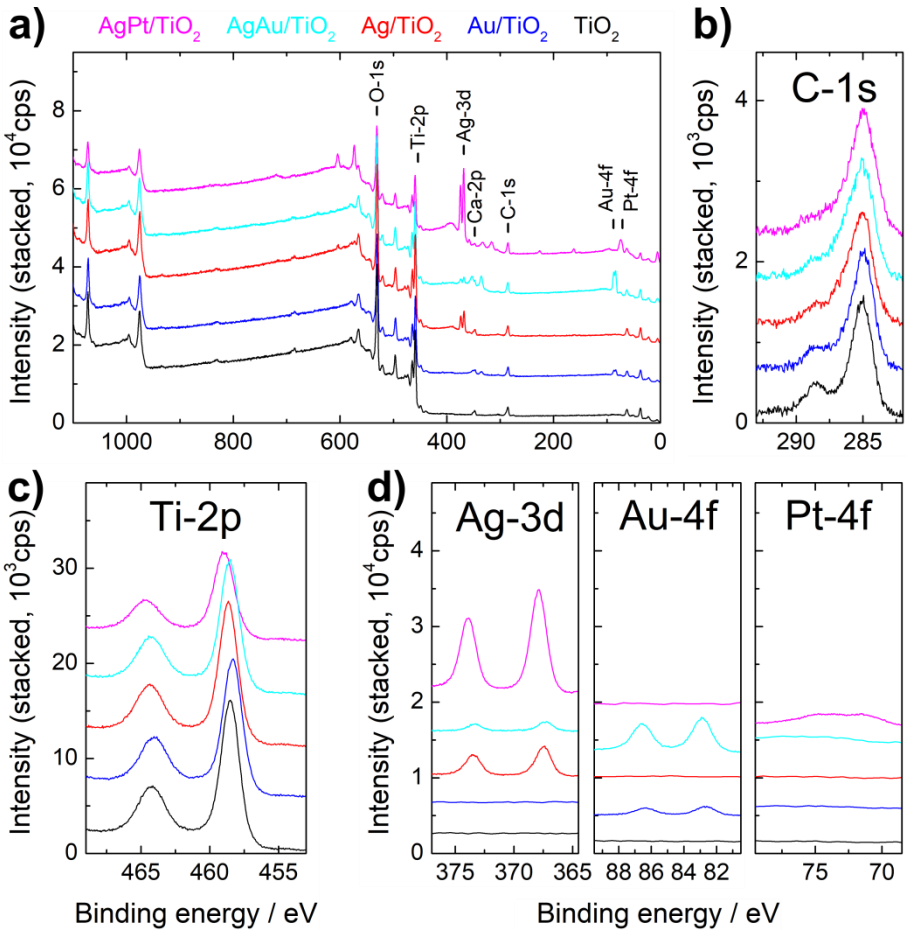

Figure 5. XPS spectra of TiO_2 nanocomposites decorated with AgPt NPs (magenta lines), AgAu NPs (cyan lines), Ag NPs (red lines), Au NPs (blue lines) and the undecorated TiO_2 thin film (black lines); a) overview spectra; b) high resolution spectra of C-1s line; c) high resolution spectra of Ti-2p lines; d) detailed spectra of the noble metals corresponding to the NPs.

In order to obtain additional information on the impact of post deposition heat treatment on the spray coated TiO_2 thin film, we performed XPS investigations. The XPS spectra of an as grown TiO_2 thin film as well as for thin films annealed at 600°C and 625°C respectively are

shown in **Figure 6**. In addition to Ti and O from the spray coated thin films and C from atmospheric contamination, e.g. by carbohydrates, the spectra also indicate the presence of Ca. The occurrence of Ca can be attributed to the use of a Ca-containing glass as substrate for the TiO_2 deposition. The signal of Ca is basically identical for the as grown as well as the annealed TiO_2 layers. Accordingly, the transport of Ca towards the surface of the spray coated TiO_2 thin film has to have happened in the initial stage of spray coating and is not an effect of the post deposition heat treatment. From the high resolution spectra of the Ti-2p and O-1s lines can also be concluded, that there is no significant change in peak positions due to annealing. The position of the Ti-$2p_{3/2}$ line is located around 458.3 eV, which is in good agreement with Ti^{4+} in TiO_2 [33,47].

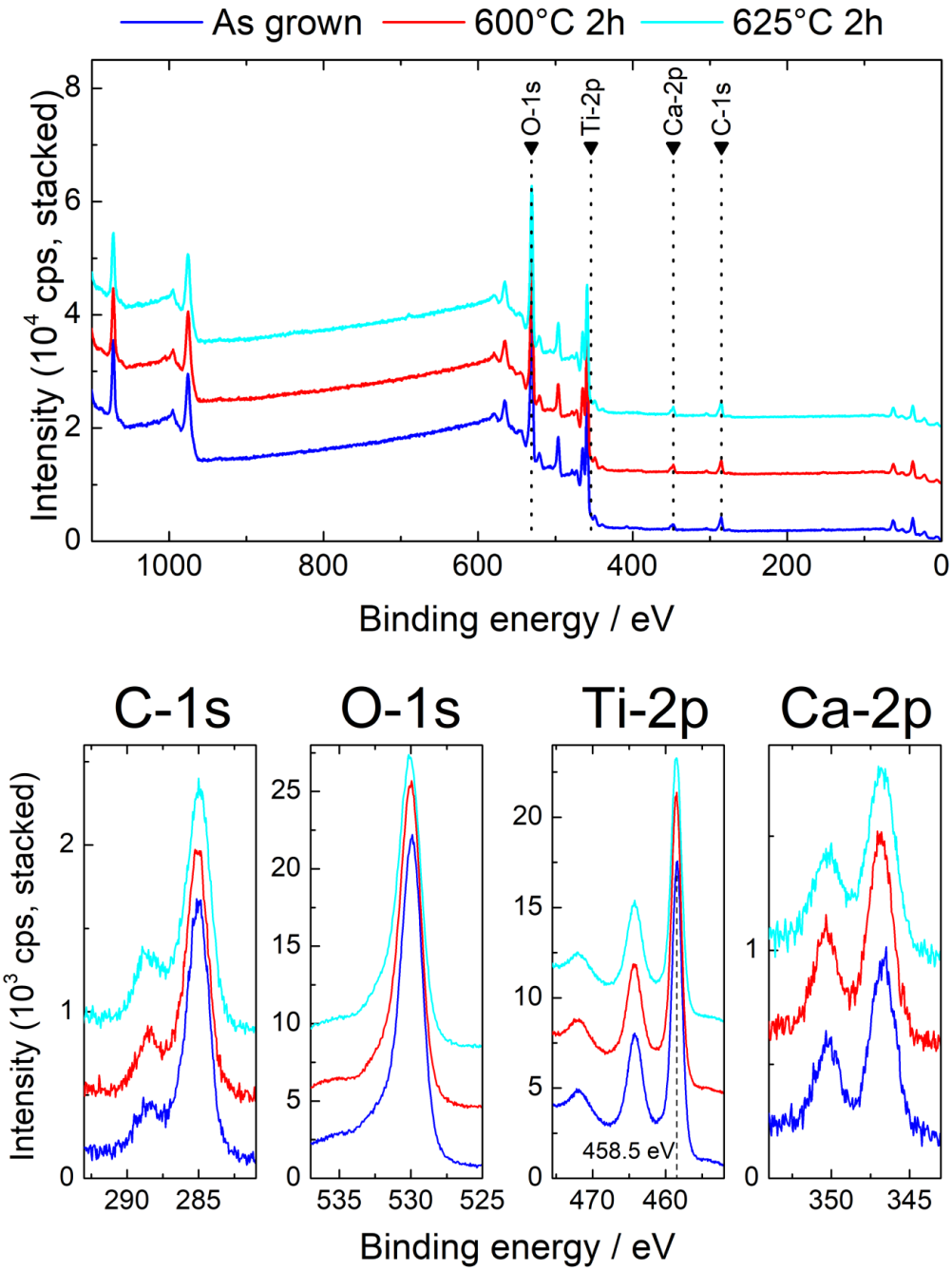

Figure 6. XPS spectra of spray coated TiO_2 thin films with different heat treatments: as grown (bottom, blue lines), annealed at 600°C for 2h (middle, red lines) and annealed at 625°C for 2h (top, cyan lines); Top row: overview spectra; Bottom row: high resolution spectra of C-1s line, O-1s line, Ti-2p lines and Ca-2p lines.

3.5. Gas sensing studies.

In order to study the response of the films to different gasses and vapors, the electrical resistances of the sensor samples were measured in the temperature range of 25°C - 400°C at std. room conditions, under the presence of gases/vapors and again rechecked under std. room conditions. A positive relation between the response for gases and vapors and the operating temperatures (OPT) was found. Reasonable OPTs for the investigated oxides lie above 250°C, which means sensing in a high temperature environments [49,50]. The optimal OPT depends on various factors, including film thickness, coverage of the surface and the porosity [50]. The conductometric method explains the gas response (changes in electrical resistance) of TiO_2 nanostructured films under the exposure to test gases in the OPT range of 200-400°C. During the sensor measurements changes in the type of conductivity were found, the majority was *n*-type electrical behavior for different gasses. For the *n*-type behavior (in case of H_2 gas testing), the gas response was calculated as follows [3]:

$$(S_n = \frac{R_{air} - R_{gas}}{R_{air}} * 100\%) \quad (3)$$

where R_{air} and R_{gas} represent the electrical resistances in air and under the test gas atmosphere, respectively. In case of exposure to the test gas, the electrical resistances decreases, that is typical for *n*-type semiconducting oxides.

Figure 7a presents the gas response versus the operating temperature of a 12 nm TiO_2 thin film sensor, thermally annealed at 625°C for 2 h in air, at four different OPTs, namely 250, 300, 350 and 400°C [3]. It is evident that the response to H_2 gas is over proportional high with respect to different types of volatile organic compounds, especially at an OPT of 350°C the big

difference in response makes the it somewhat “quasi-selective”. In **Figure 7b,c** the gas sensing results of TiO_2 thin film sensors with a thickness of 20 nm and 40 nm with TA at 600°C for 1 h at different OPTs are depicted. At an OPT of 350°C, the TiO_2 films with 12, 20 and 40 nm showed a response of ~ 25%, ~ 150% and ~ 650%, respectively. Inside the investigated temperature regimes, the optimal operating temperature for thinner structures lies between 350°C - 400°C and is hereby comparable with those reported for H_2 sensors based on TiO_2 nanostructures [14]. The highest gas response was obtained for TiO_2 layers with 40 nm thickness and thermal annealing at 600°C for 1h. In this case, the gas response is ~ 650%, which is higher compared to the reported results based on TiO nanoparticles [51].

Figure S5a shows radar plots of the response of 12 nm thick TiO_2 thin films (sprayed0.5), TA for 2 h at 625°C in air, - based sensors at three different operating temperatures. It can be seen that samples are best performing for H_2 gas sensing at an OPT of 350-400°C. **Figure S5b** presents gas response versus operating temperature of 20 nm thick TiO_2 thin films (sprayed1), TA for 1 h at 600°C in air [3]. It is evident that samples are not as selective as the 12 nm samples to H_2 gas with respect to different types of volatile organic compounds, but the response to H_2 gas is higher (about 2X). **Figure S5c** shows radar plot of the response of the 40 nm thick TiO_2 nanostructured thin films (sprayed2) which were annealed for 1 h at 600°C in air, for three different operating temperatures, namely in range 200-300°C. Thus, at an OPT of 300°C the spray1(20 nm) and spray2(40 nm) samples perform better than the spray0.5 sample (12 nm). Also it can be concluded, the samples are more selective in the OPT range 250°C - 300°C [3]. It is evident that samples with a thickness of 40 nm are quite selective to H_2 gas with respect to different types of volatile organic compounds and the gas response to H_2 is much higher compared to the thinner samples (12 and 20 nm).

ollu

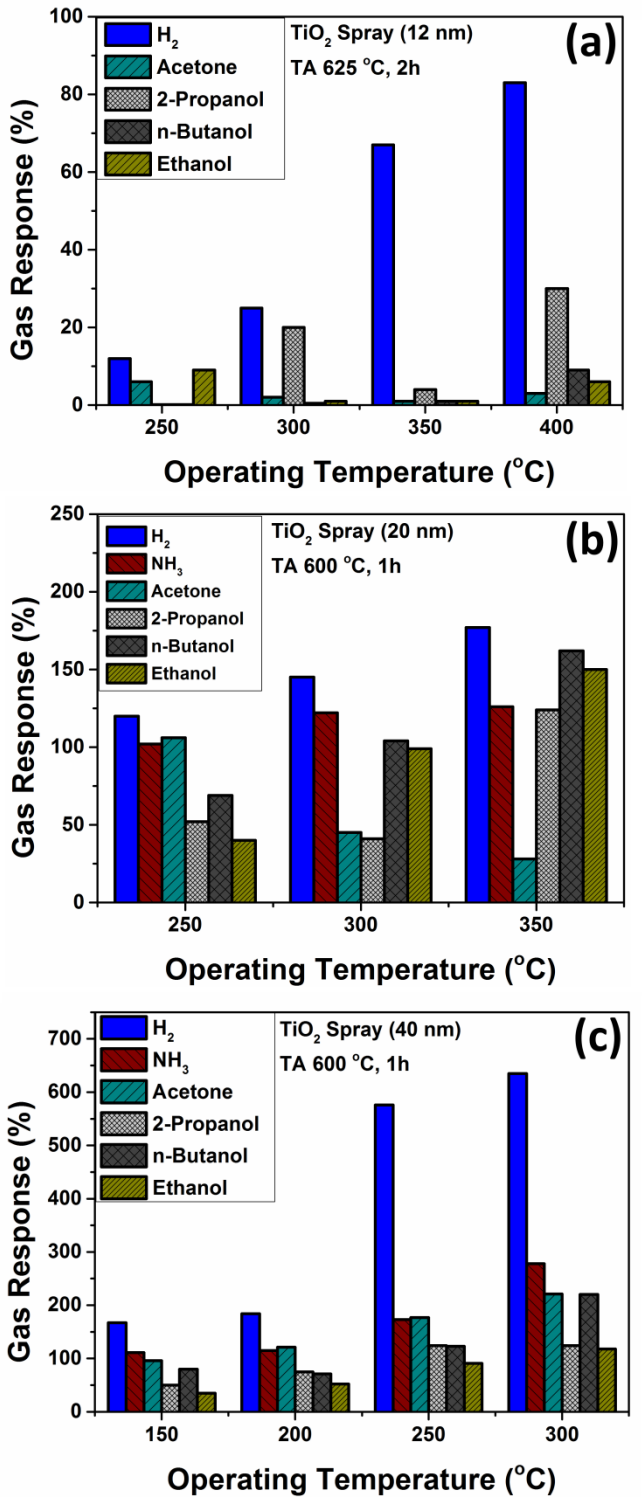

Figure 7. Gas response versus operating temperature of sprayed TiO_2 nanostructured thin film based sensors with a thickness of: **(a)** 12 nm, annealed at 625°C for 2 h in air; **(b)** 20 nm and **(c)** 40 nm, annealed at 600°C for 1 h.

An important feature for such investigations is the reproducibility and stability of the sensor structures which was observed at different OPT and gas concentrations.

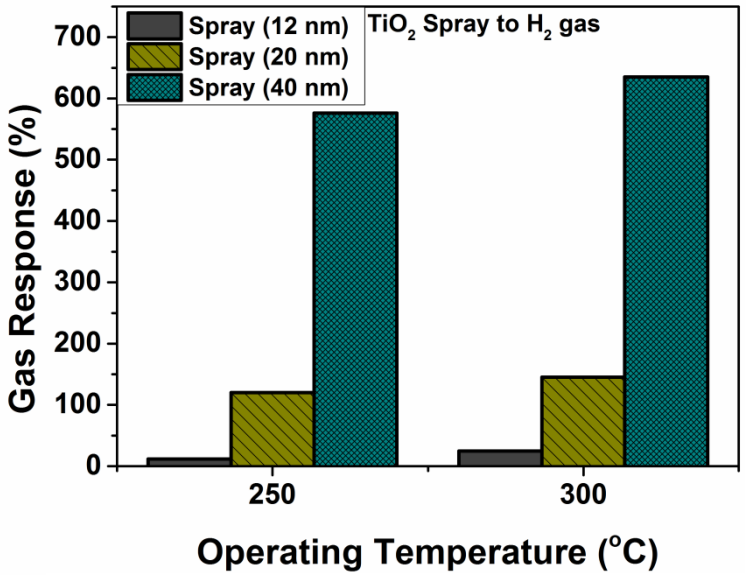

Figure 8. Comparison of responses to H_2 gas for all types of sprayed TiO_2 nanostructured thin films (12, 20 and 40 nm, respectively) - based sensors at operating temperature of 250°C and 300°C; All samples were thermal annealed at 600°C for 1 h in air. (12, 20 nm to 100 ppm, and 40 nm to 1000 ppm) (Gap size of 1 mm).

Figure 8 presents a comparison of the gas responses to H_2 gas for sprayed TiO_2 nanostructured thin films, TA at 600°C for 1 h in air, with different thicknesses, namely 12, 20 and 40 nm to H_2 gas at OPTs of 250°C and 300°C. It can be seen that the samples with a thickness of 40 nm are most sensitive to H_2 gas with a response >640% to H_2 gas at an OPT of 300°C.

Next, we are comparing only the most sensitive films (40 nm) to different gases and volatile organic compounds (H_2 gas, NH_3 vapor, and volatile organic compounds - Acetone, 2-Propanol, *n*-Butanol and Ethanol) to identify their behavior to various environments. **Figure 9** presents gas responses for the best performing TiO_2 thin film (40 nm) to H_2, NH_3, and volatile

organic compounds such as Acetone, 2-Propanol, *n*-Butanol and Ethanol at an OPT of 250°C with a response of R=580% (**Figure 9a**) and at 300°C with a response of 640% (**Figure 9b**) to a 20 s long pulse 1000 ppm of H_2 gas. Evidently the samples are semi-selective to H_2 gas with respect to others investigated under the same conditions.

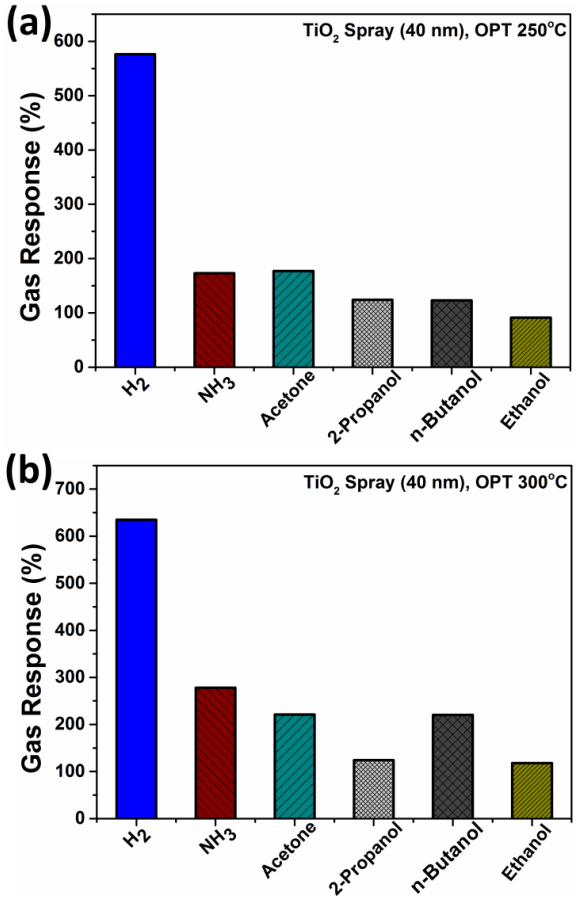

Figure 9. Gas response for TiO_2 thin films (40 nm) - based sensor structures to H_2 gas, NH_3 vapor, and volatile organic compounds, namely Acetone, 2-Propanol, *n*-Butanol and Ethanol at operating temperatures of: **(a)** 250°C; and **(b)** 300°C. All samples were thermally annealed for 1 h at 600°C in air.

The dynamic response to 1000 ppm of H_2 gas of TiO_2 films with 20 nm and 40 nm thickness is presented in **Figure 10(a-b)** at two different operating temperatures: 250°C (**Figure 10(a)**) and 300°C (**Figure 10(b)**). The calculated response and recovery times are presented in **Table S1**.

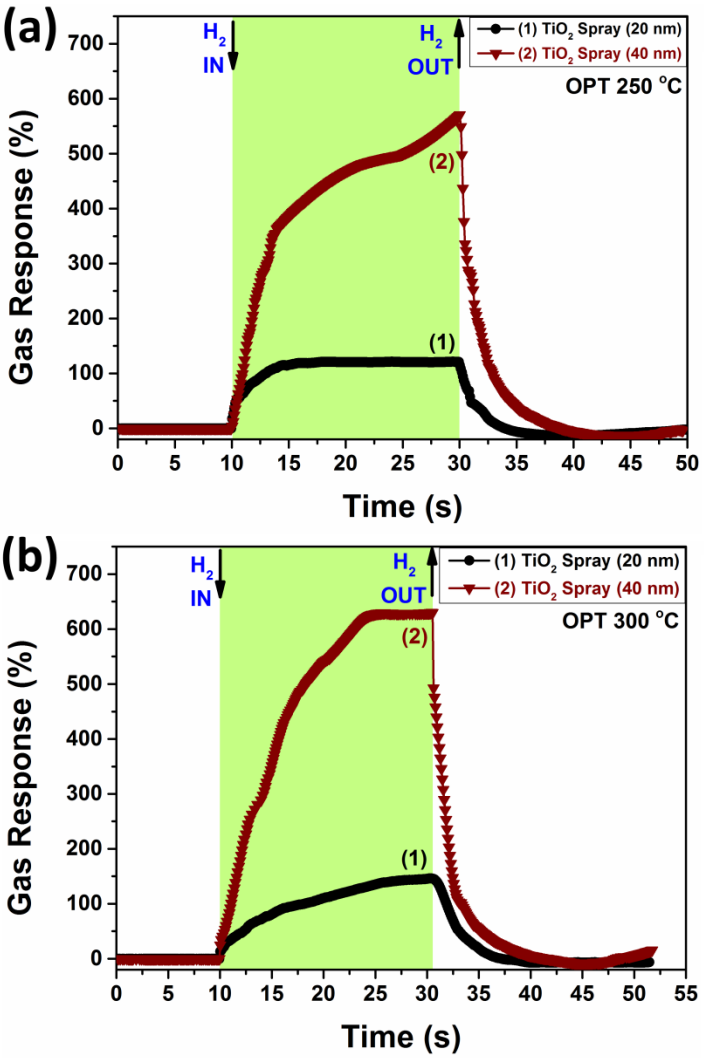

Figure 10. Dynamic gas-sensing transients to 1000 ppm of H_2 gas of a TiO_2 (20 nm) thin film **(a)**; and the TiO_2 (40 nm) **(b)** thin film based sensors at two different operating temperatures: 250°C **(a)**; and 300°C **(b)**. These nanostructured samples were thermally annealed at 600°C for 1 h in air.

The lowest response and recovery times were observed for the spray2 (40 nm) samples at an OPT 250°C (15.42 s and 3.9 s, respectively), while for the 40 nm sample at an OPT of 300°C the response and recovery times are 11.05 s and ~ 3.79 s, respectively. This can be related to a higher influence of the electron depleted top layer on the gas response.

The 20 nm samples showed a response of about 150% and the 40 nm samples of 640% at an OPT of 300°C (**Figure 10(b)**).

3.6. Gas sensing studies. Effect of noble metal nanoparticles or nanoclusters

The effect of noble metal nanoparticles or nanoclusters on gas sensing performances of nanostructured TiO_2 films ranging from 12 to 40 nm were investigated next. It is important to find approaches which allow reducing OPT and to make films much more selective or to tune it from one gas to another one or to VOC. In such a way it will be possible to control the gas response value and to fabricate different sensors based on the same material and in same technological process, just by functionalizing its surface with different types of noble nanoparticles.

For sensors with a *n*-type response (in test case with H_2, 2-Propanol, *n*-Butanol and Ethanol), formula (2) ($S_n = \frac{R_{air}-R_{gas}}{R_{air}} * 100\%$) was used since the electrical resistance of the sensor was decreasing, which is typical for semiconducting oxides with *n*-type of conductivity. The *p*-type response behavior was observed for vapors (namely, NH_3 and Acetone) and in such a case formula [3] were used:

$$(S_p = \frac{R_{gas}-R_{air}}{R_{air}} * 100\%) \quad (4)$$

since resistance was increasing when the test gas was introduced into the test chamber [52–54].

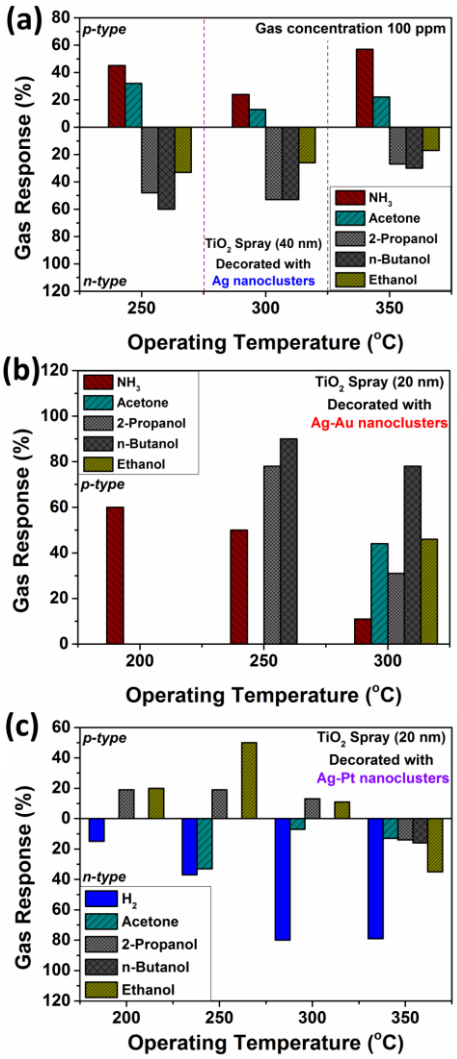

Figure 11. The gas response versus operating temperature of TiO_2 thin films: **(a)** with a thickness of 40 nm (annealed at 600°C for 1 h in air) and decorated with Ag nanoclusters; **(b)** with a thickness of 20 nm and decorated with noble Ag-Au nanoclusters; **(c)** with a thickness of 20 nm and decorated with Ag-Au nanoclusters. These samples were annealed at 600°C for 1 h in air.

According to **Figure 11a** we can conclude that *n*-type response behavior of the conductivity was observed for *n*-butanol, 2-propanol and ethanol vapors, since the electrical resistance was decreasing, but for NH_3 and acetone vapors it was increasing, analog to *p*-type behavior. Thus, by Ag NPs-decoration of the TiO_2 films (Ag-NPs@TiO_2) we can tune the gas

response from H_2 gas to *n*-butanol and 2-propanol vapors with *n*-type response behavior. It can be recommended that such Ag-NPs@TiO_2 films could be very good candidates for *n*-butanol (C_4H_9OH) detection, which is a "fusel alcohols" and extremely wide used in food industry (butter, cream, fruit, rum, whiskey, ice cream and ices, candy, baked goods and cordials) [55], as well as in a in a wide range of consumer product [56], as well as for other industrial processes [57]. Butanol is considered as a potential biofuel (butanol fuel), but n-butanol presents a moderate fire hazard With a flash point of 35 °C [58]. An increase in response to 2-propanol vapors was observed with increasing OPT from 250 to 300°C according to Figure 10a. Here, it is important to mention that isopropyl alcohol (IUPAC name 2-propanol) is a structural isomer of propanol the molecular formula C_3H_7OH, which has threshold limit of 400 ppm for short term exposure [59]. Exposure of higher concentration of 2-propanol leads to low blood pressure, dizziness, nausea and coma, etc. [59,60], hence, it is highly important to detect 2-propanol for health and safety issues. It is of great importance to mention that the detection and control of such VOCs is of great demand for various applications, e.g. detection of butanol or methanol leaks in various industrial processes [55,59–62]. The detection of methanol was possible due to fact that it reacts with oxygen over metal oxides to give oxidation and dehydration products [63]. Thus, the composition of Ag-NPs@TiO_2 films mixed oxides seem to change the surface activity of and reaction products, making it more sensitive to 2-propanol and *n*-butanol vapors.

For the thinner Ag-Au decorated TiO_2 films (Ag-Au-NPs@TiO_2) (20 nm, **Fig. 11b**), *p*-type response to 2-propanol and *n*-butanol vapors was observed, since the resistance was increasing when gas was introduced into the test chamber [52–54]. A decrease in response to ammonia vapors was observed with increasing OPT from 200 to 300°C. According to **Figure 11b** at an OPT of 200°C, there is only a NH_3 response, but at an OPT of 250°C the response to 2-Propanol, *n*-Butanol appears. Such an Ag-Au-NPs@TiO_2 can be a very good and selective

sensor to ammonia at OPT of 200°C, but with increasing OPT at an OPT of 300°C all gases lead to a response. Thus, to have the highest response and selectivity to NH_3, the OPT should be set to 200°C. A higher response to *n*-butanol vapors was observed at 250°C, but more selective with respect to other VOCs at 300°C for Ag-Au-NPs@TiO_2 films (20 nm).

According to our experimental results for Ag-Pt-NPs-functionalized TiO_2 (Ag-Pt-NPs@TiO_2) samples presented in **Figure 11c** at an OPT of 300°C, there is only a higher response to H_2 (≈80%) with *n*-type response behavior in comparison with samples functionalized with Ag or Ag-Au. With increasing OPTs, the response to 2-Propanol, *n*-Butanol starts to appear. It is clearly evident that such Ag-Pt-NPs TiO_2 films are good candidates for selective H_2 gas sensor at an OPT of 300-350°C.

Interestingly the conductivity behavior for 2-Propanol and ethanol is decreasing at OPT temperatures > 225°C-250°C until a sign change can be seen at an OPT of 350°C. This seems to be an of the effect differing conductivity mechanisms in the multicomponent films. Such Ag-Pt-NPs TiO_2 films could be candidates for selective ethanol vapor sensor at an OPT of 250°C with *p*-type behavior.

At an OPT of 350°C with *n*-type response behavior, which was of *p*-type response behavior up to OPT of 300°C, and the same can be seen for samples functionalized with Ag-Pt where disappear response to NH_3.

3.7. UV detection studies. Effect of noble metal nanoparticles or nanoclusters

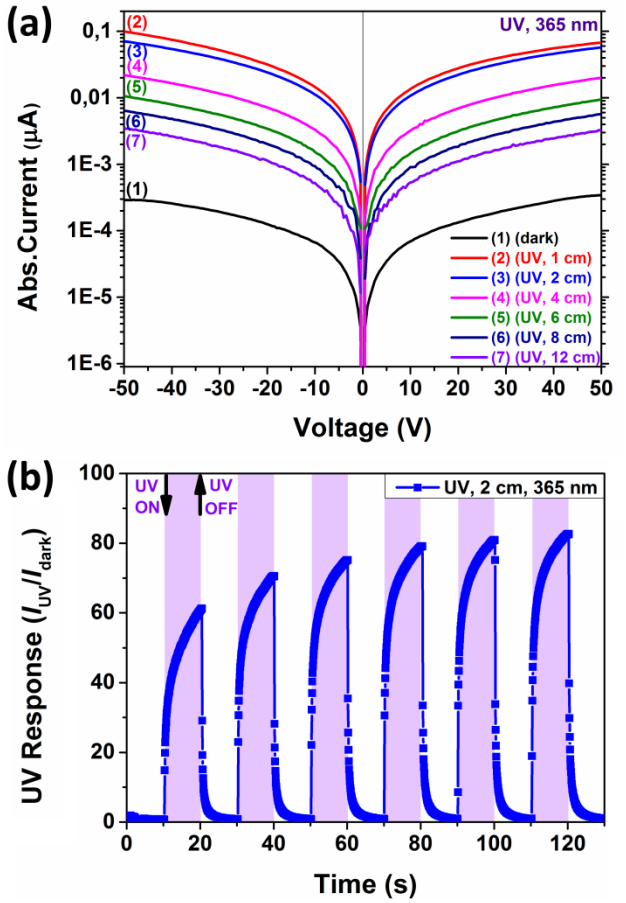

Figure 12. (a) Current – voltage curves of TiO_2 Spray 2 (40 nm) ultra-thin films measured in dark and under UV at different intensities at room temperature. These samples were thermally annealed at 600°C for 1 h in air. **(b)** The dynamic UV response to pulse durations (10 s) of a 40 nm sprayed TiO_2 sample and a bias voltage of 10 V. These samples were thermally annealed at 600°C for 1 h in air.

Figure 12a shows the current – voltage characteristics in the range of -50 V up to +50 V of a TiO_2 thin film with a thickness of 40 nm in dark and under UV (365 nm) illumination at different light intensities (varied by the distance from the source to sample). Experiments confirmed as expected, that the thinner films have a higher resistance, since the electrical

resistivity (ρ) of thin films is dependent on the thickness ($\rho = R_S t$, where R_S is the sheet resistance and t is the thickness of film) [64]. A slight non-linear characteristic can be seen which may indicate on formation of Schottky contacts.

In **Figure 12b** the dynamic response of TiO_2 films (40 nm) to UV (365 nm, 2 cm distance) at room temperature, sample was TA at 600°C for 1 h at an applied bias voltage of 10 V. The response to UV radiation was defined as: $S = (I_{UV} / I_{dark})$, and it was found to be ≈ 82 with response and recovery times τ_{r1}=0.1 s, τ_{r2}=2.96 s and τ_{d1}=0.16 s, τ_{d1}=1.51 s, respectively.

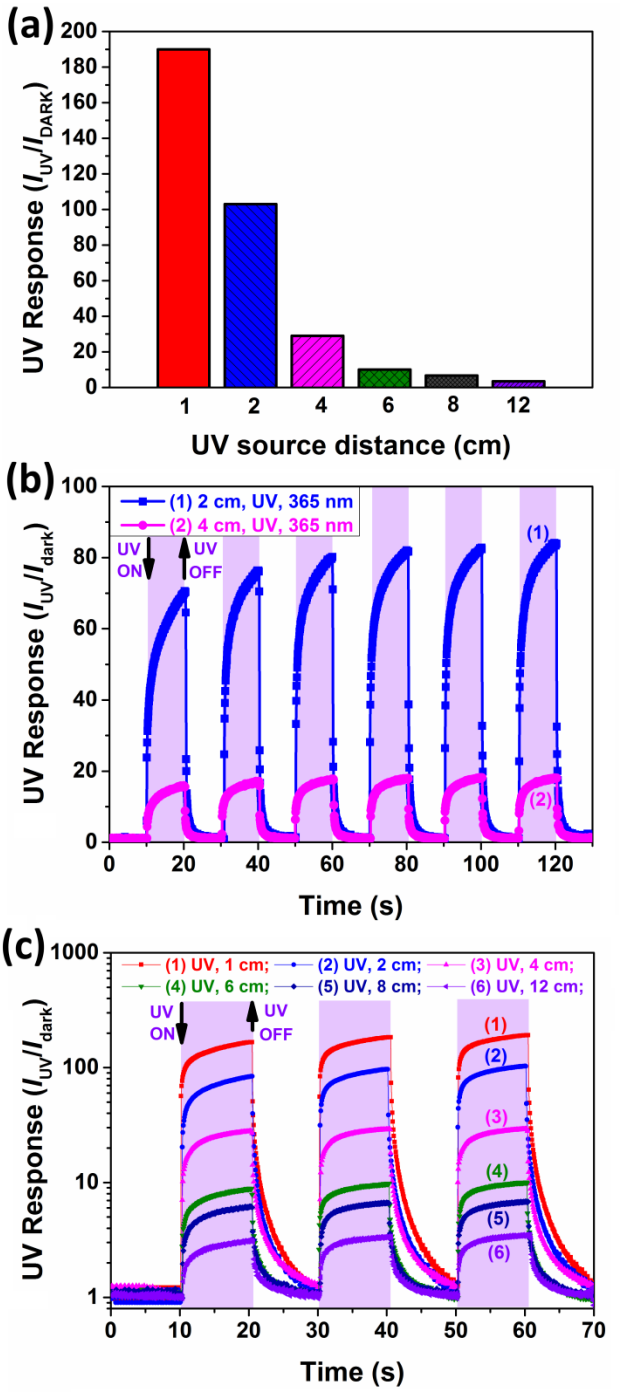

Figure 13. **(a)** Response to UV intensity adjusted by the distance of the source to the sample. TiO_2 Spray (40 nm) + Au nanoparticles, TA 600ºC for 1 h at an applied bias voltage of 50 V; **(b)** Dynamic response to UV (365 nm, at two different distances 2 cm and 4 cm) of TiO_2 Spray (40 nm), TA 600°C for 1 h at an applied bias voltage of 10 V; **(c)** Dynamic response to UV

(365 nm, at different distances 1 cm – 12 cm) of TiO_2 Spray (40 nm) + Au nanoparticles, TA 600°C for 1 h at applied bias voltage of 50 V.

In **Figure 13a** the response to UV radiation at a bias voltage of 50 V of the 40 nm sample TiO_2 (Spray (40 nm), TA 600°C for 1 h) is presented. It can be seen that the response decreases considerable if the distance is increasing. **Figure 13b** presents the dynamic responses to UV (at two different distances 2 cm and 4 cm) of TiO_2 film with 20 nm thickness (Spray1), TA at 600°C for 1h at an applied bias voltage of 10 V. The UV response at a distance of 2 cm is ≈ 82 with response/recovery times of τ_{r1}=0.1 s, τ_{r2}=2.96 s and τ_{d1}=0.16 s, τ_{d2}=1.51 s, respectively, and at the distance of 4 cm response is ≈ 17 with response/recovery times of τ_{r1}=0.34 s, τ_{r2}=4.11 s and τ_{d1}=0.09s, τ_{d2}=1.13s, respectively. We can clearly see that the sensor structure is changing its response in dependence of UV source sensor distance. In **Figure 13c** the dynamic response to UV (365 nm, at different distances 1 cm – 12 cm) is shown of a TiO_2 Spray (40 nm), TA 600°C for 1 h at applied bias voltage of 50 V at room temperature. The response/recovery times for samples investigated in **Figure 13** are summarized in Table 1.

Table 1. Response/recovery times for Au-nanoparticles@TiO_2 Spray (40 nm), TA 600°C for 1 h at applied bias voltage of 50 V.

	τ_{r1} (s)	τ_{r2} (s)	τ_{d1} (s)	τ_{d1} (s)
TA600_1h_Au_50V_Sample 3+UV10_1cm	0.14	4.32	0.05	0.8
TA600_1h_Au_50V_Sample 3+UV10_2cm	0.11	3.27	0.05	0.85
TA600_1h_Au_50V_Sample 3+UV10_4cm	0.18	2.93	0.13	1.88
TA600_1h_Au_50V_Sample 3+UV10_6cm	0.22	3.09	0.3	2.61
TA600_1h_Au_50V_Sample 3+UV10_8cm	0.14	2.76	0.24	2.05
TA600_1h_Au_50V_Sample 3+UV10_12cm	0.32	3.65	0.16	1.91

3.8. Gas and UV sensing mechanism. Effect of noble metal nanoparticles or nanoclusters

Adsorbed oxygen on the surface of the TiO_2 ultra-thin films extracts free electrons from it and transforms into oxygen species, depending strongly on the OPT value [65–67].

$$O_{2(gas)} \leftrightarrow O_{2(ads)}^{----} \quad (5)$$

$$O_{2(ads)} + e^- \rightarrow O_2^-{}_{(ads)} \quad (6)$$

$$O_{2(ads)}^- + e^- \leftrightarrow 2O_{(ads)}^- \quad (7)$$

$$O_{(ads)}^- + e^- \leftrightarrow O_{(ads)}^{2-} \quad (8)$$

The roles of different types of oxygen species adsorbed on the sensor surface are determined for various TiO_2 ultra-thin films. When the sensor is exposed to the gas environment, H_2 molecules are adsorbed on the film surface and react with adsorbed oxygen species which act as active sites for gas to get attached, thus detection takes places, as follows [68]:

$$H_2 + \frac{1}{2}O_{2(ads)}^- \rightarrow H_2O + e^- \quad (9)$$

$$H_2 + O_{(ads)}^- \rightarrow H_2O + e^- \quad (10)$$

This will also reduce the width of the depletion region, which leads to a change in the electrical resistance of the TiO_2 films during the detection process. The reaction is exothermic (1.8 kcal.mol-1) [69], that will lead to quick desorption of water molecules from the surface of TiO_2 films.

The 40 nm film shows the highest response to H_2 gas at 300°C mainly due because O_2- species are predominantly adsorbed on the film surface and the interaction of these with test gas.

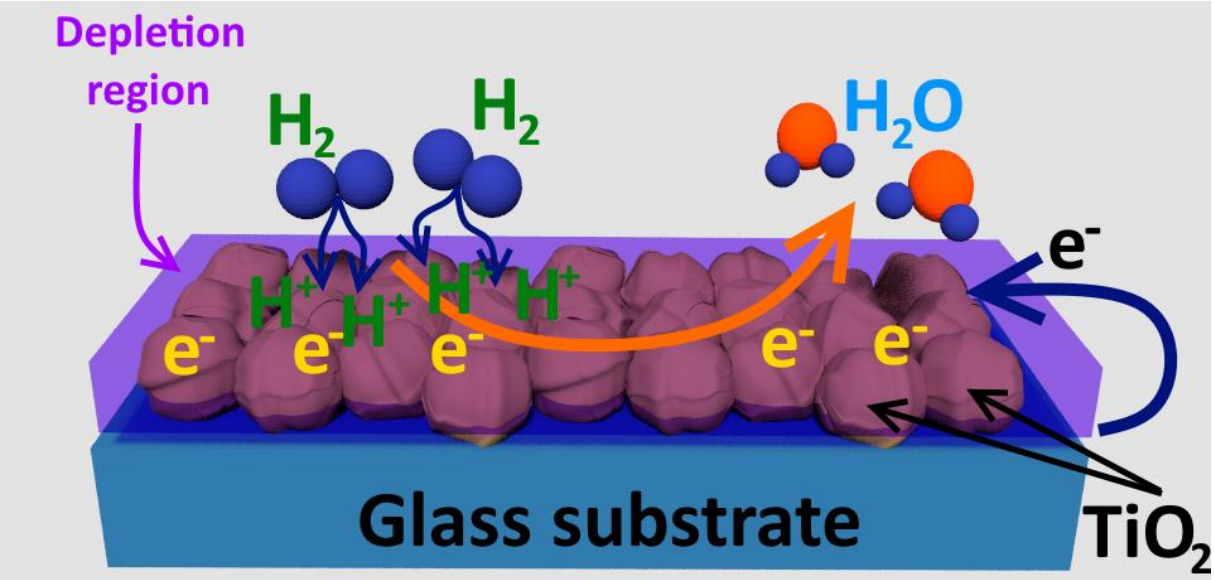

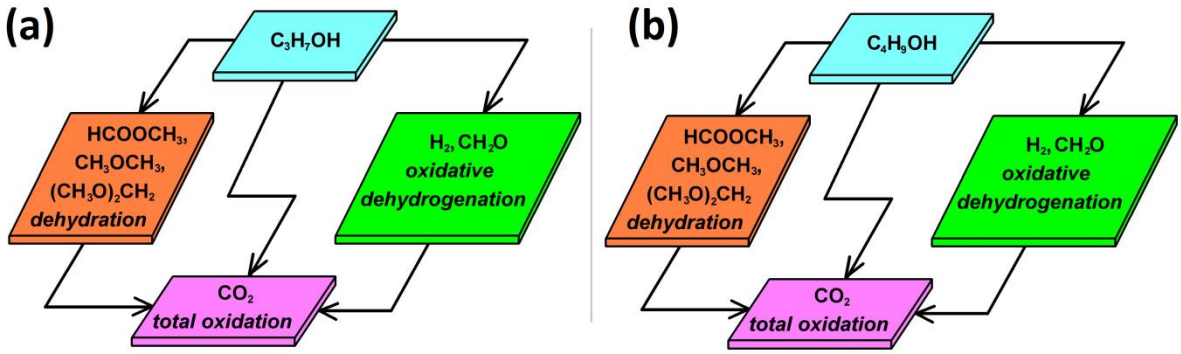

Sheme 1. Reaction pathway for the oxidation process of of AgO/TiO_2 surfaces of developed sensor structures.

Scheme 1 shows the detection pathway of methanol up to final product formed after oxidation of the reactions of intermediates [61].

During the exposure of Ag/TiO_2 or Ag-Au/TiO_2 surfaces with *n*-butanol vapor, it reacts with oxygen species to form CO_2 and H_2O. The electrons will be released from oxygen species and will reduce the sizes of the depletion region and of a potential barrier. This process induces an increase in conductivity and may be described as follows [70–72]:

$$(C_4H_9OH)_{gas} \leftrightarrow (C_4H_9OH)_{ads} \quad (11)$$

$$(C_4H_9OH)_{ads} + 12O^{2-}_{ads} \rightarrow 4CO_2 + 5H_2O + 24e^- \quad (12)$$

$$(C_4H_9OH)_{ads} + 12O^{-}_{ads} \rightarrow 4CO_2 + 5H_2O + 12e^- \quad (13)$$

These discussions indicate on the gas sensing superiority of TiO_2 nanocrystalline films. It concludes that a large surface area due to crystals will provide a larger active sites and favors gas-oxide reaction and it will rich pores and perform diffusions of test gas, which in final will enhance gas response.

The proposed vapor sensing between 2-Propanol and TiO_2 surface is described as follows [59,60]:

$$2C_3H_8O + 9[O^-_{2(ads)}] \rightarrow 6CO_2 \uparrow + 8H_2O \uparrow + 9e^- \downarrow \quad (14)$$

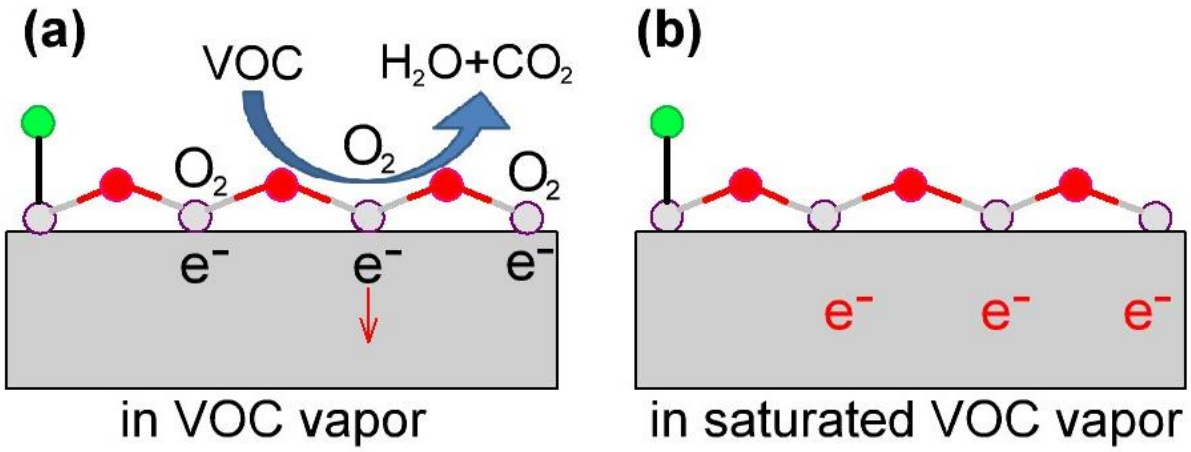

Scheme 2. Schematic diagram of the hydrogenation process of TiO_2 films of sensing mechanism on mixed phases TiO_2 surface. The black e^- and red e^- are electrons adsorbed on surface and released, respectively.

Since 2-Propanol is a reducing vapor, then it will be oxidized to CO_2, H_2O and release of electrons into films.

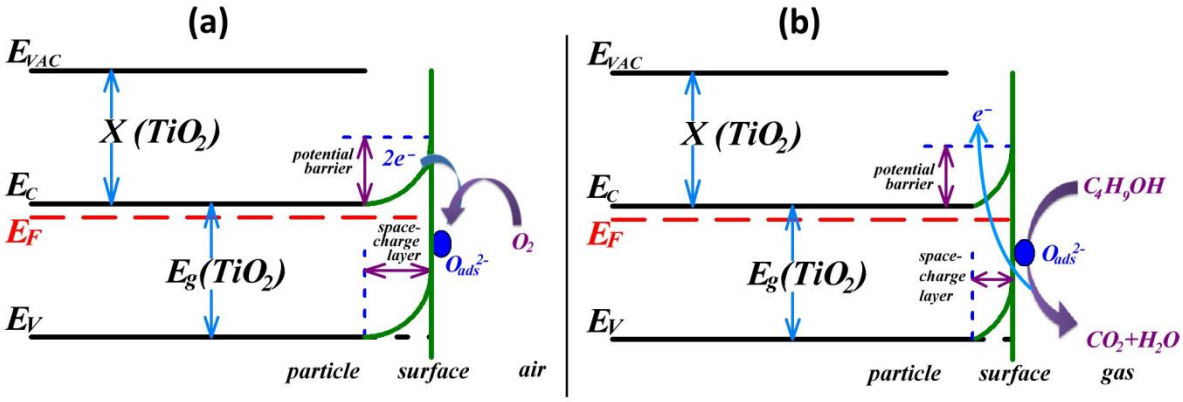

Figure 14. **(a)** Energy band diagrame of TiO_2 in air; **(a)** Energy band diagrame of TiO_2 in VOC.

Conclusions

TiO_2 thin films with quite smooth surface and crystalline phase anatase have been deposited on glass by spray pyrolysis of an aerosol based on titanium diisopropoxide, acetylacetone and

isopropanol. From the morphological and AFM studies, it can be concluded that the growth approach (by spraying and subsequent annealing) is quite attractive for sensor applications due to their granular view. Different thick (12, 20 and 40 nm) TiO_2 nanocrystalline thin films have been sprayed and their morphological, structural, electrical and gas sensing performances have been characterized. It was found that the film thickness in this investigated region has a great effect on their characteristics and gas sensing performances. For sensors based on the TiO_2 with a thickness of 20 nm, after TA 625°C for 1 h, it is possible to change the selectivity from one gas to another (see **Figure S5a**) by changing the OPT as follows:

a) To obtain an ethanol sensor the OPT of 300°C is necessary;
b) To obtain a 2-Propanol sensor the OPT should be 350°C;
c) To obtain an Acetone sensor the OPT should be 400°C;

Considering that for H_2 gas the electrical behavior is of *n*-type, we can consider that such sensor structures are always selective to H_2 gas with respect to VOCs, which shows *p*-type behavior during detections.

The gas response of TiO_2 ultra-thin films towards H_2 gas was studied, we observed that 40 nm thick films, thermally annealed at 600°C for 1 h, are a good candidates for H_2 sensor. Thus, the current work explored the possibility to detect gasses using optimally prepared TiO_2 ultra-thin films.

The functionalization of TiO_2 films with Ag, Au, Ag-Au and Ag-Pt allows controlling their selectivity from one gas/vapor to another as well as the type of conductivity as follows:

a) TiO_2 Spray (40 nm) films with Ag nanoparticles showed two types of conductivity, namely NH_3, -Acetone with *p-type* and for 2-Propanol, *n*-Butanol and Ethanol with *n-type* behavior, and are more selective to *n*-Butanol at OPT of 250 ^oC *n-type* behavior,

as well as selective to NH_3 at all OPT with *p-type* behavior. Here, if we would consider *p-type* and *n-type* behavior then the sensors show very good selectivity to NH_3 and *n*-Butanol;

b) TiO_2 Spray (20 nm) films functionalized with Ag-Au nanoparticles showed only *p-type* behavior and are selective to NH_3 at an OPT of 200°C, but with increasing OPTs, the sensor becomes more sensitive to 2-Propanol, *n*-Butanol, Acetone and Ethanol with selectivity to *n*-Butanol.

c) TiO_2 Spray (12 nm) films functionalized with Au nanoparticles showed only *n-type* behavior. At an OPT of 250 °C the response to *n*-Butanol disappears and 2-Propanol sensing is possible.

d) High selectivity and response to H_2 gas was achieved using 40 nm TiO_2 thin films decorated with noble metal nanoclusters. The synergetic effect of the catalytic nanoclusters Ag, Au and Pt top layers promotes their selectivity.

e) TiO_2 spray 2 (40 nm) films are very good as H_2 gas sensor after thermal annealing at 600°C for 1 h with a response (>580%) which is several times higher than for 20 nm thick films at OPT of 250°C ((>110%)), at relatively low operating temperature.

f) At an OPT of 300°C the TiO_2 spray 1 (20 nm) films show a response of >150% to H_2 gas

g) At an OPT of 300°C the TiO_2 spray 2 (40 nm) films show a response of >640% to H_2 gas.

The developed sensor structures and their production procedure is quite attractive for various industrial applications to detect leakage of gases and/or VOCs.

ACKNOWLEDGEMENTS

This research was funded in part by the German Research Foundation (DFG- Deutsche Forschungsgemeinschaft) under the schemes FOR 2093 & SFB 1261 (AD 183/17-1). O.L. acknowledges the Alexander von Humboldt Foundation for the research fellowship for experienced researchers (3-3MOL/1148833 STP) at the Institute for Materials Science, Kiel University, Germany. This research was in part supported by the STCU within the Grant 6229.

REFRENCES

[1] A. V Singhal, H. Charaya, I. Lahiri, Noble Metal Decorated Graphene-Based Gas Sensors and Their Fabrication: A Review, Crit. Rev. Solid State Mater. Sci. 42 (2017) 499–526. doi:10.1080/10408436.2016.1244656.

[2] A.M. Azad, S.A. Akbar, S.G. Mhaisalkar, L.D. Birkefeld, K.S. Goto, Solid-State Gas Sensors: A Review, J. Electrochem. Soc. . 139 (1992) 3690–3704. http://jes.ecsdl.org/content/139/12/3690.abstract.

[3] O. Lupan, V. Cretu, V. Postica, O. Polonskyi, N. Ababii, F. Schütt, V. Kaidas, F. Faupel, R. Adelung, Non-planar nanoscale p–p heterojunctions formation in ZnxCu1−xOy nanocrystals by mixed phases for enhanced sensors, Sensors Actuators B Chem. 230 (2016) 832–843. doi:https://doi.org/10.1016/j.snb.2016.02.089.

[4] M. Hoppe, N. Ababii, V. Postica, O. Lupan, O. Polonskyi, F. Schütt, S. Kaps, L.F. Sukhodub, V. Sontea, T. Strunskus, F. Faupel, R. Adelung, (CuO-Cu2O)/ZnO:Al heterojunctions for volatile organic compound detection, Sensors Actuators B Chem. 255 (2018) 1362–1375. doi:https://doi.org/10.1016/j.snb.2017.08.135.

[5] B. Bourrounet, T. Talou, A. Gaset, Application of a multi-gas-sensor device in the meat industry for boar-taint detection, Sensors Actuators B Chem. 27 (1995) 250–254. doi:https://doi.org/10.1016/0925-4005(94)01596-A.

[6] O. Lupan, V. Postica, R. Adelung, F. Labat, I. Ciofini, U. Schürmann, L. Kienle, L. Chow, B. Viana, T. Pauporté, Functionalized Pd/ZnO Nanowires for Nanosensors, Phys. Status Solidi – Rapid Res. Lett. 12 (n.d.) 1700321. doi:10.1002/pssr.201700321.

[7] V. Postica, F. Schütt, R. Adelung, O. Lupan, Schottky Diode Based on a Single Carbon–Nanotube–ZnO Hybrid Tetrapod for Selective Sensing Applications, Adv. Mater. Interfaces. 4 (2017) 1700507. doi:10.1002/admi.201700507.

[8] O. Lupan, V. Postica, F. Labat, I. Ciofini, T. Pauporté, R. Adelung, Ultra-sensitive and selective hydrogen nanosensor with fast response at room temperature based on a single Pd/ZnO nanowire, Sensors Actuators B Chem. 254 (2018) 1259–1270. doi:https://doi.org/10.1016/j.snb.2017.07.200.

[9] G.F. Fine, L.M. Cavanagh, A. Afonja, R. Binions, Metal Oxide Semi-Conductor Gas Sensors in Environmental Monitoring, Sensors. 10 (2010) 5469–5502. doi:10.3390/s100605469.

[10] S. Wu, Z. Weng, X. Liu, K.W.K. Yeung, P.K. Chu, Functionalized TiO2 Based Nanomaterials for Biomedical Applications, Adv. Funct. Mater. 24 (n.d.) 5464–5481. doi:10.1002/adfm.201400706.

[11] Y.-K. Jun, H.-S. Kim, J.-H. Lee, S.-H. Hong, High H2 sensing behavior of TiO2 films formed by thermal oxidation, Sensors Actuators B Chem. 107 (2005) 264–270.

doi:https://doi.org/10.1016/j.snb.2004.10.010.
[12] M.F. Bin Alam, D.-T. Phan, G.-S. Chung, Palladium nanocubes decorated on a one-dimensional ZnO nanorods array for use as a hydrogen gas sensor, Mater. Lett. 156 (2015) 113–117. doi:https://doi.org/10.1016/j.matlet.2015.05.007.
[13] D. Sett, D. Basak, Highly enhanced H2 gas sensing characteristics of Co:ZnO nanorods and its mechanism, Sensors Actuators B Chem. 243 (2017) 475–483. doi:https://doi.org/10.1016/j.snb.2016.11.163.
[14] A. Monamary, K. Vijayalakshmi, Highly sensitive hydrogen sensor based on nickel incorporated TiO2 nanostructures operating at room temperature, J. Mater. Sci. Mater. Electron. 29 (2018) 5316–5326. doi:10.1007/s10854-017-8497-7.
[15] N. Chen, D. Deng, Y. Li, X. Liu, X. Xing, X. Xiao, Y. Wang, TiO2 nanoparticles functionalized by Pd nanoparticles for gas-sensing application with enhanced butane response performances, Sci. Rep. 7 (2017) 7692. doi:10.1038/s41598-017-08074-y.
[16] A.L. Linsebigler, G. Lu, J.T. Yates, Photocatalysis on TiO2 Surfaces: Principles, Mechanisms, and Selected Results, Chem. Rev. 95 (1995) 735–758. doi:10.1021/cr00035a013.
[17] C. Xiang, Z. She, Y. Zou, J. Cheng, H. Chu, S. Qiu, H. Zhang, L. Sun, F. Xu, A room-temperature hydrogen sensor based on Pd nanoparticles doped TiO2 nanotubes, Ceram. Int. 40 (2014) 16343–16348. doi:https://doi.org/10.1016/j.ceramint.2014.07.073.
[18] I. Alhomoudi, J. Thakur, R. Naik, G. Auner, G. Newaz, Anatase TiO2 films based CO gas sensor: Film thickness, substrate and temperature effects, Appl. Surf. Sci. 253 (2007) 8607–8614.
[19] C. Hornbostel, Construction materials : types, uses, and applications / Caleb Hornbostel, Wiley, New York, 1978.
[20] T. Mazza, E. Barborini, P. Piseri, P. Milani, D. Cattaneo, A. Li Bassi, C.E. Bottani, C. Ducati, Raman spectroscopy characterization of TiO2 rutile nanocrystals, Phys. Rev. B. 75 (2007) 45416. doi:10.1103/PhysRevB.75.045416.
[21] U. Diebold, The surface science of titanium dioxide, Surf. Sci. Rep. 48 (2003) 53–229. doi:https://doi.org/10.1016/S0167-5729(02)00100-0.
[22] T. Mazza, E. Barborini, I.N. Kholmanov, P. Piseri, G. Bongiorno, S. Vinati, P. Milani, C. Ducati, D. Cattaneo, A.L. Bassi, C.E. Bottani, A.M. Taurino, P. Siciliano, Libraries of cluster-assembled titania films for chemical sensing, Appl. Phys. Lett. 87 (2005) 103108. doi:10.1063/1.2035874.
[23] N. Savage, B. Chwieroth, A. Ginwalla, B.R. Patton, S.A. Akbar, P.K. Dutta, Composite n–p semiconducting titanium oxides as gas sensors, Sensors Actuators B Chem. 79 (2001) 17–27. doi:https://doi.org/10.1016/S0925-4005(01)00843-7.
[24] N.O. Savage, S.A. Akbar, P.K. Dutta, Titanium dioxide based high temperature carbon monoxide selective sensor, Sensors Actuators B Chem. 72 (2001) 239–248. doi:https://doi.org/10.1016/S0925-4005(00)00676-6.
[25] H.P. Maruska, A.K. Ghosh, Photocatalytic decomposition of water at semiconductor electrodes, Sol. Energy. 20 (1978) 443–458. doi:https://doi.org/10.1016/0038-092X(78)90061-0.
[26] B. Karunagaran, P. Uthirakumar, S.J. Chung, S. Velumani, E.-K. Suh, TiO2 thin film gas sensor for monitoring ammonia, Mater. Charact. 58 (2007) 680–684. doi:https://doi.org/10.1016/j.matchar.2006.11.007.
[27] J. Moon, H.-P. Hedman, M. Kemell, A. Tuominen, R. Punkkinen, Hydrogen sensor of Pd-decorated tubular TiO2 layer prepared by anodization with patterned electrodes on SiO2/Si substrate, Sensors Actuators B Chem. 222 (2016) 190–197. doi:https://doi.org/10.1016/j.snb.2015.08.054.
[28] T. Torimoto, Y. Ohta, K. Enokida, D. Sugioka, T. Kameyama, T. Yamamoto, T. Shibayama, K. Yoshii, T. Tsuda, S. Kuwabata, Ultrathin oxide shell coating of metal

nanoparticles using ionic liquid/metal sputtering, J. Mater. Chem. A. 3 (2015) 6177–6186. doi:10.1039/C4TA06643J.
[29] X. Bévenot, A. Trouillet, C. Veillas, H. Gagnaire, M. Clément, Hydrogen leak detection using an optical fibre sensor for aerospace applications, Sensors Actuators B Chem. 67 (2000) 57–67. doi:https://doi.org/10.1016/S0925-4005(00)00407-X.
[30] S. Zeng, K.-T. Yong, I. Roy, X.-Q. Dinh, X. Yu, F. Luan, A Review on Functionalized Gold Nanoparticles for Biosensing Applications, Plasmonics. 6 (2011) 491. doi:10.1007/s11468-011-9228-1.
[31] P. Wang, Z. Shao, M. Ulfa, T. Pauporté, Insights into the Hole Blocking Layer Effect on the Perovskite Solar Cell Performance and Impedance Response, J. Phys. Chem. C. 121 (2017) 9131–9141. doi:https://doi.org/10.1021/acs.jpcc.7b00979.
[32] H. Haberland, M. Karrais, M. Mall, Y. Thurner, Thin films from energetic cluster impact: A feasibility study, J. Vac. Sci. Technol. A Vacuum, Surfaces, Film. 10 (1992) 3266–3271. doi:10.1116/1.577853.
[33] J.F. Moulder, W.F. Stickle, P.E. Sobol, K.D. Bomben, Handbook of X-ray Photoelectron Spectroscopy (Perkin-Elmer, Eden Prairie, MN, 1992), Google Sch. (2002) 128.
[34] O. Polonskyi, T. Peter, A.M. Ahadi, A. Hinz, T. Strunskus, V. Zaporojtchenko, H. Biederman, F. Faupel, Huge increase in gas phase nanoparticle generation by pulsed direct current sputtering in a reactive gas admixture, Appl. Phys. Lett. 103 (2013) 33118. doi:10.1063/1.4816036.
[35] A. Vahl, J. Strobel, W. Reichstein, O. Polonskyi, T. Strunskus, L. Kienle, F. Faupel, Single target sputter deposition of alloy nanoparticles with adjustable composition via gas aggregation cluster source, Nanotechnology. 28 (2017).
[36] Here we can cite the work on Ag nanoparticles on ZnO:Fe, (n.d.).
[37] O. Lupan, V. Postica, N. Wolff, O. Polonskyi, V. Duppel, V. Kaidas, E. Lazari, N. Ababii, F. Faupel, L. Kienle, R. Adelung, Localized Synthesis of Iron Oxide Nanowires and Fabrication of High Performance Nanosensors Based on a Single Fe2O3 Nanowire, Small. 13 (2017) 1602868. doi:10.1002/smll.201602868.
[38] O. Lupan, V. Cretu, V. Postica, M. Ahmadi, B.R. Cuenya, L. Chow, I. Tiginyanu, B. Viana, T. Pauporté, R. Adelung, Silver-doped zinc oxide single nanowire multifunctional nanosensor with a significant enhancement in response, Sensors Actuators B Chem. 223 (2016) 893–903. doi:https://doi.org/10.1016/j.snb.2015.10.002.
[39] X.H. Yang, Z. Li, G. Liu, J. Xing, C. Sun, H.G. Yang, C. Li, Ultra-thin anatase TiO2 nanosheets dominated with {001} facets: thickness-controlled synthesis{,} growth mechanism and water-splitting properties, CrystEngComm. 13 (2011) 1378–1383. doi:10.1039/C0CE00233J.
[40] T. Ohsaka, F. Izumi, Y. Fujiki, Raman spectrum of anatase, TiO2, J. Raman Spectrosc. 7 (1978) 321–324. doi:10.1002/jrs.1250070606.
[41] M. Enachi, O. Lupan, T. Braniste, A. Sarua, L. Chow, Y.K. Mishra, D. Gedamu, R. Adelung, I. Tiginyanu, Integration of individual TiO2 nanotube on the chip: Nanodevice for hydrogen sensing, Phys. Status Solidi – Rapid Res. Lett. 9 (2015) 171–174. doi:10.1002/pssr.201409562.
[42] M. Lubas, J.J. Jasinski, M. Sitarz, L. Kurpaska, P. Podsiad, J. Jasinski, Raman spectroscopy of TiO2 thin films formed by hybrid treatment for biomedical applications, Spectrochim. Acta Part A Mol. Biomol. Spectrosc. 133 (2014) 867–871. doi:https://doi.org/10.1016/j.saa.2014.05.045.
[43] O. Toshiaki, I. Fujio, F. Yoshinori, Raman spectrum of anatase, TiO2, J. Raman Spectrosc. 7 (n.d.) 321–324. doi:10.1002/jrs.1250070606.
[44] A. Nakaruk, D. Ragazzon, C.C. Sorrell, Anatase–rutile transformation through high-temperature annealing of titania films produced by ultrasonic spray pyrolysis, Thin

Solid Films. 518 (2010) 3735–3742. doi:https://doi.org/10.1016/j.tsf.2009.10.109.
[45] I. Lukačević, S.K. Gupta, P.K. Jha, D. Kirin, Lattice dynamics and Raman spectrum of rutile TiO2: The role of soft phonon modes in pressure induced phase transition, Mater. Chem. Phys. 137 (2012) 282–289. doi:https://doi.org/10.1016/j.matchemphys.2012.09.022.
[46] O. Frank, M. Zukalova, B. Laskova, J. Kurti, J. Koltai, L. Kavan, Raman spectra of titanium dioxide (anatase, rutile) with identified oxygen isotopes (16, 17, 18), Phys. Chem. Chem. Phys. 14 (2012) 14567–14572. doi:10.1039/C2CP42763J.
[47] C. Powell, NIST X-ray Photoelectron Spectroscopy Database, NIST Standard Reference Database Number 20, National Institute of Standards and Technology, Gaithersburg MD, 20899 (2000), doi:10.18434/T4T88K, (retrieved 2018-02-08)., (1989). doi:10.18434/t4t88k.
[48] Y. Tian, T. Tatsuma, Mechanisms and Applications of Plasmon-Induced Charge Separation at TiO2 Films Loaded with Gold Nanoparticles, J. Am. Chem. Soc. 127 (2005) 7632–7637. doi:10.1021/ja042192u.
[49] A. Maity, S.B. Majumder, NO2 sensing and selectivity characteristics of tungsten oxide thin films, Sensors Actuators B Chem. 206 (2015) 423–429. doi:https://doi.org/10.1016/j.snb.2014.09.082.
[50] P. Wang, Z. Shao, M. Ulfa, T. Pauporté, Insights into the Hole Blocking Layer Effect on the Perovskite Solar Cell Performance and Impedance Response, J. Phys. Chem. C. 121 (2017) 9131–9141. doi:10.1021/acs.jpcc.7b00979.
[51] W. Chomkitichai, N. Tamaekong, C. Liewhiran, A. Wisitsoraat, S. Sriwichai, S. Phanichphant, H2 Sensor Based on Au/TiO2 Nanoparticles by Flame-Made, Eng. J. 16 (2012). doi:https://doi.org/10.4186/ej.2012.16.3.135.
[52] O. Lupan, V. Postica, J. Gröttrup, A.K. Mishra, N.H. de Leeuw, R. Adelung, Enhanced UV and ethanol vapour sensing of a single 3-D ZnO tetrapod alloyed with Fe2O3 nanoparticles, Sensors Actuators B Chem. 245 (2017) 448–461. doi:https://doi.org/10.1016/j.snb.2017.01.107.
[53] O. Lupan, F. Schütt, V. Postica, D. Smazna, Y.K. Mishra, R. Adelung, Sensing performances of pure and hybridized carbon nanotubes-ZnO nanowire networks: A detailed study, Sci. Rep. 7 (2017) 14715. doi:10.1038/s41598-017-14544-0.
[54] O. Lupan, V. Postica, J. Gröttrup, A.K. Mishra, N.H. de Leeuw, J.F.C. Carreira, J. Rodrigues, N. Ben Sedrine, M.R. Correia, T. Monteiro, V. Cretu, I. Tiginyanu, D. Smazna, Y.K. Mishra, R. Adelung, Hybridization of Zinc Oxide Tetrapods for Selective Gas Sensing Applications, ACS Appl. Mater. Interfaces. 9 (2017) 4084–4099. doi:10.1021/acsami.6b11337.
[55] R.L. Hall, R.L. Oser, J.J. Broderick, F. Brumburgh, A.T. Fiore, C.E. Fricke, L.F. Hasnaw, D. Jorysch, J.K. Krum, J.L. Laughlin, R. V. Leary, J.R. Leitz, J.H. McClumphy, J.F. Perkins, M.F. Preisner, A.T. Schramm, F.R. Schumm, R.C. Sherwood, H.C. Spencer, A.S. Wendt, Recent Progress in the Consideration of Flavoring Ingredients Under the Food Additives Amendment III GRAS Substances, J. Food Technol. (1965).
[56] Environmental Health Criteria monograph No. 65, Geneva: World Health Organization, in: Butanols Four Isomers, 1987.
[57] I. Mellan, Industrial Solvents, New York Van Nostrand Reinhold. (1950) 482–488.
[58] "NIOSH Pocket Guide to Chemical Hazards #0076". National Institute for Occupational Safety and Health (NIOSH), (n.d.). https://www.cdc.gov/niosh/npg/npgd0076.html.
[59] P.S. Karthikeyan, P. Dhivya, P.D. Raj, M. Sridharan, V2O5 thin film for 2-Propanol vapor sensing, Mater. Today Proc. 3 (2016) 1510–1516. doi:https://doi.org/10.1016/j.matpr.2016.04.035.

[60] Y.L. Wu, Q. Luan, S.J. Chang, Z. Jiao, W.Y. Weng, Y.H. Lin, C.L. Hsu, Highly Sensitive beta-Ga2O3 Nanowire Nanowires Isopropyl Alcohol Sensor, IEEE Sens. J. 14 (2014) 401–405. doi:10.1109/JSEN.2013.2283885.
[61] G. Neri, A. Bonavita, G. Rizzo, S. Galvagno, S. Capone, P. Siciliano, Methanol gas-sensing properties of CeO2–Fe2O3 thin films, Sensors Actuators B Chem. 114 (2006) 687–695. doi:https://doi.org/10.1016/j.snb.2005.06.062.
[62] N.A. Beckers, M.T. Taschuk, M.J. Brett, Selective room temperature nanostructured thin film alcohol sensor as a virtual sensor array, Sensors Actuators B Chem. 176 (2013) 1096–1102. doi:https://doi.org/10.1016/j.snb.2012.09.041.
[63] J.M. Tatibouët, Methanol oxidation as a catalytic surface probe, Appl. Catal. A Gen. 148 (1997) 213–252. doi:https://doi.org/10.1016/S0926-860X(96)00236-0.
[64] I.E. Stewart, M.J. Kim, B.J. Wiley, Effect of Morphology on the Electrical Resistivity of Silver Nanostructure Films, ACS Appl. Mater. Interfaces. 9 (2017) 1870–1876. doi:10.1021/acsami.6b12289.
[65] N. Yamazoe, J. Fuchigami, M. Kishikawa, T. Seiyama, Interactions of tin oxide surface with O2, H2O AND H2, Surf. Sci. 86 (1979) 335–344. doi:https://doi.org/10.1016/0039-6028(79)90411-4.
[66] S. Chang, Oxygen chemisorption on tin oxide: Correlation between electrical conductivity and EPR measurements, J. Vac. Sci. Technol. 17 (1980) 366–369. doi:10.1116/1.570389.
[67] S. Lenaerts, J. Roggen, G. Maes, FT-IR characterization of tin dioxide gas sensor materials under working conditions, Spectrochim. Acta Part A Mol. Biomol. Spectrosc. 51 (1995) 883–894. doi:https://doi.org/10.1016/0584-8539(94)01216-4.
[68] O. Lupan, V. V Ursaki, G. Chai, L. Chow, G.A. Emelchenko, I.M. Tiginyanu, A.N. Gruzintsev, A.N. Redkin, Selective hydrogen gas nanosensor using individual ZnO nanowire with fast response at room temperature, Sensors Actuators B Chem. 144 (2010) 56–66. doi:https://doi.org/10.1016/j.snb.2009.10.038.
[69] S. Basu, A. Dutta, Room-temperature hydrogen sensors based on ZnO, Mater. Chem. Phys. 47 (1997) 93–96. doi:https://doi.org/10.1016/S0254-0584(97)80035-1.
[70] M. Kanerva, L.-S. Johansson, J.M. Campbell, H. Revitzer, E. Sarlin, T. Brander, O. Saarela, Hydrofluoric–nitric–sulphuric-acid surface treatment of tungsten for carbon fibre-reinforced composite hybrids in space applications, Appl. Surf. Sci. 328 (2015) 418–427. doi:https://doi.org/10.1016/j.apsusc.2014.12.036.
[71] X. Liu, N. Chen, X. Xing, Y. Li, X. Xiao, Y. Wang, I. Djerdj, A high-performance n-butanol gas sensor based on ZnO nanoparticles synthesized by a low-temperature solvothermal route, RSC Adv. 5 (2015) 54372–54378. doi:10.1039/C5RA05148G.
[72] Y. V Kaneti, Q.M.D. Zakaria, Z. Zhang, C. Chen, J. Yue, M. Liu, X. Jiang, A. Yu, Solvothermal synthesis of ZnO-decorated [small alpha]-Fe2O3 nanorods with highly enhanced gas-sensing performance toward n-butanol, J. Mater. Chem. A. 2 (2014) 13283–13292. doi:10.1039/C4TA01837K.